3 Star Formation in Galaxies

Samuel Boissier
Laboratoire d'Astrophysique de Marseille, Université Aix-Marseille & CNRS, UMR7326, Marseille cedex 13, France

T.D. Oswalt, W.C Keel (eds.), *Planets, Stars and Stellar Systems. Volume 6: Extragalactic Astronomy and Cosmology*, DOI 10.1007/978-94-007-5609-0_3,

Abstract: The process of star formation is at the core of the evolutionary cycle of galaxies, as newborn stars produce new chemical elements, dust, and light. The energetic output delivered first by stellar winds and then by supernovae a few Myr after a star formation episode may also directly impact on the evolution of galaxies and their interstellar medium (ISM), as well as having an effect on the intergalactic medium (IGM), through feedback and outflows.

This chapter concerns star formation on galactic scales. First, the galactic processes that may affect large-scale star formation are presented. Second, the various methods to measure star formation rates are discussed (star formation tracers, timescales, calibrations, limits). Finally, the observational status concerning star formation in galaxies (its relation to other quantities and its evolution) is presented. The Schmidt Law (star formation rate–gas relationship) is amply discussed.

Keywords: Dust extinction, Evolution, Galaxy, Initial Mass Function, Schmidt Law, Star formation, Star formation diagnostics, Star formation history, Star formation rate, Star formation threshold, Star formation tracers, Toomre parameter

List of Abbreviations: *FIR*, Far infrared; *GMC*, Giant molecular clouds; *IGM*, Intergalactic medium; *IMF*, Initial mass function; *ISM*, Interstellar medium; *SFH*, Star formation history; *SFR*, Star formation rate; *SSFR*, Specific star formation rate; *YSO*, Young stellar objects

1 Introduction

Star formation is at the core of the cycle of evolution of galaxies. From their gas reservoir (and its replenishment), stars are formed at a given rate (the star formation rate, SFR) with a paramount impact on many aspects of galaxy evolution. The first one is the simple fact that galaxies are filled with stars that emit the light that allows us to see them. Generations after generations, the most massive of newly formed stars will also quickly yield the chemical elements formed in their core (stellar nucleosynthesis) to enrich the interstellar medium (ISM). This chemical enrichment will affect the properties and evolution of the next generations of stars and allow in fact the galaxies to hosts planets and life itself (both relying on heavy elements). Star formation is important for other aspects of extragalactic physics: the energy released by evolved stars and supernovae can affect the interstellar medium. It may heat the gas and prevent the collapse of the gas or, on the contrary, shock it and induce the formation of new stars. Its role on the distribution of stars and gas impacts the morphology of galaxies. Star formation finally affects the intergalactic medium (IGM), as winds due to violent episodes of star formation may exit their original galaxy and chemically and dynamically impact the IGM.

Because star formation is so crucial in shaping the galaxies (and maybe even their surroundings) the way they are seen, the subject has naturally motivated a lot of work. While it is generally admitted that stars form within molecular clouds, in the densest phases of the interstellar gas, the complex details of the process are not yet fully understood. For the actual physics of star formation, on small scales, the reader is referred to Chap. 3 of this handbook, or the McKee and Ostriker (2007) review. Such studies of the details of the process are accessible mostly in the Milky Way where star formation regions can be studied in great details.

On the other hand, star formation is also related to the scales of galaxies themselves. First, from a purely observational point of view, in many cases it is only possible to know the integrated SFR for the whole galaxy. But there are also physical links to be investigated: what is the main driver of star formation on the large scales? How is the SFR related to the galaxy gas reservoir? Is the SFR affected (enhanced or reduced) by the spiral arms of disk galaxies? By the density? By the galaxy kinematics? By other phenomenon? These questions are the subject of this chapter, focused on star formation on the scales of galaxies (by opposition to the scales of individual star-forming regions).

While early on the SFR (and its history) was derived in external galaxies from global quantities such as colors (with the help of evolutionary synthesis models), a number of SFR diagnostics (based on observables that will be called "SFR tracers") have been developed and largely used since the 1980s (emission lines, UV continuum, far-infrared luminosities). SFRs are usually deduced from these tracers using famous calibrations, relying on specific physics or empirical relations that are often forgotten. None of the SFR tracers in fact provide a really instantaneous SFR. To measure it, it is assumed that the SFR was constant on a typical timescale (between a few Myr and a few 100 Myr depending on the tracer). A given initial mass function (IMF) has also to be chosen. It is important to understand the origin of the calibrations used to derive the SFR and to know the assumptions underlying them and their limits.

Early on, Schmidt (1959) found a relation between the SFR and the gas density in the Milky Way. This relation, now known as the Schmidt Law, has been revisited frequently and has taken many forms (over the scales of whole galaxies or "local" scales of a few 100 pc within galaxies). It is still today an active field of research and a constraint for models of the evolution of galaxies. Today, SFR are routinely derived for large samples of galaxies, in the nearby universe, as well as in deep fields showing us galaxies in a young universe. The SFR distribution is computed and even integrated to provide a "cosmic" SFR and its evolution: the history of star formation in the whole universe. These studies bring an unprecedented amount of information on the history of galaxies.

In this chapter, the subjects briefly described above are distributed in three sections. In Sect. 2, the formalism describing star formation is presented, followed by the theoretical ideas suggesting relations between star formation and other galactic phenomenon or quantities. The diagnostics for measuring the star formation activity in galaxies (the SFR tracers) are presented in Sect. 3 including the underlying assumptions, the calibrations, the timescales, and some observational difficulties. Finally, a review of the current observational status concerning star formation on the scales of galaxies, the Schmidt Law, the specific star formation rate, and the star formation history is proposed in Sect. 4.

Other reviews (complementary to the material presented in these pages) can be found in books and classical papers, such as Chapter 9 of Mo et al. (2009), Kennicutt (1998a), and Larson (1992). A number of ideas about star formation in galaxies were discussed during a nice international conference hold at the Abbazia di Spineto on the subject "SFR@50: Filling the Cosmos with Stars" at the occasion of the 50th birthday of the seminal paper by Schmidt (1959). While no traditional proceedings were published, the reader may find the presentations given in that occasion on DVD or via the Internet.[1]

[1] http://www.arcetri.astro.it/sfr50/index.html

2 Theoretical Background

2.1 Formalism

In order to describe star formation in quantitative terms, it is necessary to adopt a simple formalism. It would be ideal to know at any time the functional form form(m, t) describing the number of stars dN formed in the dm mass interval during the time dt so that dN = form$(m, t)dtdm$. It is convenient to decompose this functional form into two independent terms. First, the total amount of material forming stars from interstellar gas by unit of time (in, e.g., $M_\odot$ year^{-1}) is called the star formation rate (SFR, noted ψ in the following). Second, the stellar mass (m) distribution of a generation of newly formed stars (the initial mass function, IMF, noted ϕ in the following). The IMF is defined as $\phi(m) = dN/dm$ and normalized as follows:

$$\int_{M_l}^{M_u} m\phi(m)dm = 1, \tag{3.1}$$

where M_l and M_u are the lower and upper mass limits, respectively. In his classical study, Salpeter (1955) defined in fact the logarithmic IMF $\xi(m) = dN/d\log(m)$. The two functions are simply linked by $\xi(m) = ln(10)m\phi(m)$. There are some uncertainties concerning the upper and lower limits, but it is usual to consider values between 0.1 and 100 $M_\odot$. With this formalism, form$(m, t) = \psi(t)\phi(m)$, where it is implicitly assumed that the IMF is stationary in time and only dependent on m (see however, ❯ Sect. 3.8.2 for different suggestions).

The IMF is often parametrized as a power law, following the classical study of Salpeter (1955). Under this assumption, it is possible to write $\phi(m) \propto m^{-(1+x)}$ or equivalently $\xi(m) \propto m^{-x}$. The index x, measuring the logarithmic slope of the IMF, was found by Salpeter (1955) to have a value of 1.35 in the solar neighborhood. Even though it was estimated over a limited mass range, this value is still frequently used. However, more recent determination of the IMF have established that the IMF presents a flattening at low masses. The universal IMF of Kroupa (2001) is an example of formulations more in accordance with the recent measurements. It is characterized by a slope of $x = 0.3$ between 0.1 and 0.5 $M_\odot$, and $x = 1.3$ for masses larger than 0.5 $M_\odot$. In the following, this IMF (largely used in the literature) is adopted. More details on the IMF can be found elsewhere in these volumes (❯ Chap. 4 of Volume 5).

The IMF might result from fundamental physical processes (such as turbulence and self-gravity, etc.) leading to star formation. For this reason, it is reasonable to expect some level of universality, and there are indeed good signs of it (e.g., Bastian et al. 2010, and references therein), but see other considerations in ❯ Sect. 3.8.2. With a universal IMF, star formation is summarized in the SFR, which dictates how much mass is converted into stars per unit time and, as a consequence, what will be the production of heavy elements, light, feedback, etc. Understanding what influences the SFR on the scales of galaxies is thus of paramount importance for every aspect of galaxy evolution. The rest of the chapter is an attempt to summarize the present understanding of the SFR on the galactic scales.

2.2 Conditions for Star Formation

The modern view of star formation is that giant molecular clouds (GMC) are a prerequisite to form stars (e.g., Leroy et al. 2008, and references therein). Once molecular clouds are formed, "local" processes (not considered in this chapter) will transform part of them into stars,

on a short timescales (e.g., Tamburro et al. 2008). In that case, the question of star formation reduces to the formation of molecular gas and GMCs from which stars will be formed (e.g., Blitz and Rosolowsky 2006).

Many processes reviewed below have been presented as favoring the collapse or condensation of gas. In the current adopted view, they should be seen as not leading directly to the apparition of stars, but to the formation of molecular gas and molecular clouds. The processes described in the Sect. 2.2 concern conditions that should be fulfilled for star formation to occur, leading to the concept of thresholds for star formation. Section 2.3 will concern the direct influences on the SFR itself.

2.2.1 Gravitational Instability

The most obvious and discussed effect is the disk gravitational instability. In reality, other instabilities (e.g., the thermal and Parker instability, see for instance in Elmegreen 1993a) may play a role. Wang and Silk (1994) argue that the gravitational one is the leading phenomenon, with only some contribution from other instabilities, an idea frequently accepted. While studying the stability of stellar disks (in order to explain the observation of spiral and S0 galaxies with smooth distribution of stars), Toomre (1964) established that a rotating stellar disk is unstable when $Q_* < 1$, where the "Toomre parameter" Q_* is defined as

$$Q_* = \frac{\sigma_* \kappa}{3.36 G \Sigma_*}. \tag{3.2}$$

Σ_* is the stellar surface density, σ_* is the velocity dispersion, and κ is the epicyclic frequency. κ can be defined as (Binney and Tremaine 1987):

$$\kappa = \left(R \frac{d\Omega^2}{dR} + 4\Omega^2 \right)^{0.5}. \tag{3.3}$$

The Toomre parameter Q_* can be seen as the balance between the velocity dispersion and the Coriolis force tending to tear apart the stars, counterbalancing their gravity. This result inspired a lot of other works that gave to this "Toomre stability criterion" a diversity of forms. For a gaseous disk (of surface density $\Sigma_{\rm gas}$ and velocity dispersion $\sigma_{\rm gas}$), one can assume (e.g., Cowie 1981; Kennicutt 1989; Wang and Silk 1994) that the disk is unstable when $Q < 1$ where

$$Q = \frac{\sigma_{\rm gas} \kappa}{\pi G \Sigma_{\rm gas}}. \tag{3.4}$$

It is common to define a gas "critical" density $\Sigma_{\rm crit}$ such that $Q = 1$. The gaseous disk is unstable when $\Sigma_{\rm gas} > \Sigma_{\rm crit}$ following the idea of Quirk (1972). While originally, the criterion concerns axisymetric instabilities, it may also be appropriate for various processes of star formation, for instance, the collapse of expanding shells or of turbulence-compressed regions (see Elmegreen and Hunter 2006, and references therein).

In a number of studies (e.g., Kennicutt 1989; Martin and Kennicutt 2001), a pragmatic approach has been adopted by using Q' in place of Q, defined simply as

$$Q' = \alpha_Q \, Q, \tag{3.5}$$

α_Q is a normalization factor, determined by measuring the limit of the disk stability and affecting $Q' = 1$ to it. In this way, Martin and Kennicutt (2001) found $\alpha_Q = 0.69 \pm 0.2$.

Wang and Silk (1994) also proposed an approximation for the Q parameter taking into account the effect of the stellar disk (based on the analysis of two isothermal fluids in Jog and Solomon 1984) whose density can help the collapse of the gaseous component:

$$Q \simeq \frac{\sigma_{\rm gas}\kappa}{\pi G \Sigma_{\rm gas}} \left(1 + \frac{\Sigma_* \, \sigma_{\rm gas}}{\Sigma_{\rm gas} \, \sigma_*}\right)^{-1}. \tag{3.6}$$

Note that this effect of the stellar density in (3.6) can be hidden in α_Q of (3.5) that should then however depend on the stellar density.

2.2.2 Shear Criterion

Noticing that star formation seems to occur in regions of low shear, Elmegreen (1993a) proposed another definition of the Q parameter, incorporating the shear rather than the epicyclic frequency:

$$Q_A = \frac{2.5\sigma_{\rm gas} A}{\pi G \Sigma_{\rm gas}}, \tag{3.7}$$

where A is the Oort shear constant:

$$A = 0.5R\frac{d\Omega}{dR}. \tag{3.8}$$

Ω is the angular frequency. For a flat rotation curve with a constant linear velocity V (independent from the radius R), one has $\Omega = V/R$. It is easy to find that Q from (3.4) is then close to Q_A. This is true for a large part of disks in spiral galaxies, but makes differences in the inner parts of spirals and dwarf galaxies where the shear is low (Hunter et al. 1998). Seigar (2005) argued that the observed shear rates do present a threshold (at $A/\Omega \sim 0.7$) corresponding to a null star formation rate.

2.2.3 Formation of a Cold Phase

Schaye (2004) suggested that the formation of a cold phase and an efficient formation of molecular gas (depending on the physics of the ISM) is more relevant to star formation than gravitational stability effects over large scale. He found a critical surface density that depends (weakly) on the metallicity, the gas fraction, the flux of ionizing photons, and the ratio of the thermal to total pressure. He provided a fitting formula in his paper, and a typical local critical gas density $\Sigma_{\rm crit} \sim 3 - 10 {\rm M}_\odot \, {\rm pc}^{-2}$ for "reasonable values" of the parameters.

2.3 Galactic Influences on the Star Formation Rates

Many processes on galactic scales have been proposed to directly affect the star formation rate itself. The more often discussed ones are reviewed below. A comparative study of many propositions has been done recently by Leroy et al. (2008).

2.3.1 Free Fall

It is possible to write the star formation rate density in a disk as the ratio of the gas density and the timescale to turn gas into stars, with an efficiency ϵ (e.g., Wang and Silk 1994; Larson 1992):

$$\Sigma_\psi = \epsilon \frac{\Sigma_{\rm gas}}{\tau}. \tag{3.9}$$

What sets the timescale τ? The first natural idea is to consider the free fall time for pure gravitational instability that leads to $\tau \propto \rho_{\rm gas}^{-0.5}$ (e.g., Madore 1977), giving for a constant scale height of the disk (e.g., Bigiel et al. 2008; Leroy et al. 2008, and references therein):

$$\Sigma_\psi \propto \Sigma_{\rm gas}^{1.5}. \tag{3.10}$$

2.3.2 Hydrostatic Equilibrium

Contrary to the assumption in the above section, the scale height (h) of a disk might not be constant, but regulated by the hydrostatic equilibrium of the disk. It is then approximated by Corbelli (2003) as:

$$h = \frac{\sigma_{\rm gas}}{\pi G} \left(\frac{\Sigma_{\rm gas}}{\sigma_{\rm gas}} + \frac{\Sigma_*}{\sigma_*} \right)^{-1}. \tag{3.11}$$

It is still possible to use $\tau \propto \rho_{\rm gas}^{-0.5}$ with $\rho_{\rm gas} = \Sigma_{\rm gas}/2h$, leading to (see also Leroy et al. 2008):

$$\Sigma_\psi \propto \frac{\Sigma_{\rm gas}^2}{\sigma_{\rm gas}} \left(1 + \frac{\Sigma_*}{\Sigma_{\rm gas}} \frac{\sigma_{\rm gas}}{\sigma_{*,z}} \right)^{0.5} \tag{3.12}$$

In a parallel approach, Abramova and Zasov (2008) used the assumption of hydrostatic equilibrium to compute the scale height of the gaseous disk, and then use it to compute volume density. They showed that the volume density of gas and SFR correlate better than the surface densities. They also suggested a direct dependence of the SFR on the stellar surface density.

2.3.3 Gravitation Versus Dispersion

Another point of view is to consider that the perturbation growth timescale τ from (3.9) is obtained by balancing dispersion against gravitation (Larson 1992):

$$\tau \propto \frac{\sigma_{\rm gas}}{\pi G \Sigma_{\rm gas}}. \tag{3.13}$$

Assuming the velocity dispersion is constant, the star formation rate density is then

$$\Sigma_\psi \propto \Sigma_{\rm gas}^2. \tag{3.14}$$

This relation should apply to kpc scales because the gravitational aggregation proceeds on these scales.

2.3.4 Self-regulated Star Formation

When star formation occurs, it may dynamically heat the gaseous disk. Then, $\sigma_{\rm gas}$ in (3.13) is not constant (in contrast with the assumption of Sect. 2.3.3) but will increase with star formation, what will also increase the Toomre parameter Q. The disk may then become stable, star formation stops. The gas can then cool down and Q go down. Thus, it is possible to consider that Q has a quasi-constant value (around 1). Self-regulation was suggested by, e.g., Kennicutt (1989) noticing that the ratio $\Sigma_{\rm gas}/\Sigma_{\rm crit}$ presents a small variation over a large range of $\Sigma_{\rm gas}$. In that case, by combining $Q = 1$, (3.4) and (3.13), one obtains $\tau \propto \kappa^{-1}$, leading for the star formation rate (using (3.9)) to

$$\Sigma_\psi \propto \Sigma_{\rm gas}\kappa. \tag{3.15}$$

Note that for a flat rotation curve (a good approximation to observations of rotation curves in the Milky Way and nearby galaxies), $\kappa = \sqrt{2}\Omega$ so that the SFR depends in this case on the density of gas and the rotation curve, both quantities being relatively easy to observe in nearby galaxies.

Larson (1992) noted that the cases leading to (3.15) and (3.14) are two simplistic assumptions and that reality might be somewhere in between, i.e.,

$$\Sigma_\psi \propto \Sigma_{\rm gas}^{\alpha}\kappa^{\beta}; 1 < \alpha < 2; 0 < \beta < 1. \tag{3.16}$$

For a flat rotation curve, this can be written as

$$\Sigma_\psi \propto \Sigma_{\rm gas}^{\alpha}\Omega^{\beta}. \tag{3.17}$$

Note that this self-regulated form is obtained for either a constant Toomre Q (3.4) or for a constant value of the shear Toomre parameter Q_A (3.7).

2.3.5 Cloud Collapse Versus Stellar Disruption

Madore (2010) proposed that the collapse time scale for a cloud (parametrized as $\tau_C \propto \rho_{\rm gas}^{-n}$) should be combined with a timescale τ_S, characteristic of the disruptive effect of star formation (at a place in a galaxy, once stars are formed, the gas is dispersed and ionized, so that no further star formation can occur at that place for the time τ_S). The star formation rate (per volume unit) can then be written as

$$\rho_\psi \propto \frac{\rho_{\rm gas}^{n}}{\tau_S + \rho_{\rm gas}^{-n}}. \tag{3.18}$$

Madore (2010) showed that this functional form allow to reproduce the trend obtained by Bigiel et al. (2008) between the star formation rate and the total gas surface density (see Sect. 4).

2.3.6 Cloud–Cloud Collisions

Assuming that the crucial step of neutral gas turning into molecular gas (formation of GMCs) occur during cloud-cloud collisions, Wyse (1986) proposed that the star formation rate should be proportional to Σ_{HI}^2 and included a dynamical factor to take into account the effect of the spiral arms (see Sect. 2.3.8 below).

Under the assumption of cloud-cloud collisions, Tan (2000) obtained a more complex formula, including the effect of shear on the collision rate:

$$\Sigma_\psi \propto \Sigma_{\rm gas}\Omega(1-0.7\beta), \tag{3.19}$$

where $\beta = d\,ln(V)/d\,ln(R)$. Note that β is null for a flat rotation curve, in wich case the SFR law obtained has the same form as (3.17) obtained with a different approach.

2.3.7 Physics of the ISM

Since stars are formed within molecular clouds, the SFR may be directly linked to the processes affecting the amount of molecular gas present in a galaxy, i.e., to the detailed physics of the ISM. Which process actually governs the molecular fraction within galaxies is however under discussions.

Elmegreen (1993b) proposed that the fraction of molecular gas is set by the hydrostatic pressure and the radiation field and that this is the limiting factor for star formation rather than the gravitational assembly of material into clouds and GMCs. This idea was pursued by several authors (Leroy et al. 2008, and references therein). Blitz and Rosolowsky (2006) expressed it by saying that the molecular ratio $R_{\rm mol} = \Sigma_{H2}/\Sigma_{HI}$ should depend on the pressure:

$$R_{\rm mol} = (P/P0)^\alpha. \tag{3.20}$$

For low pressures ($P \ll P0$), over large part of galaxies (where HI dominates over H2), the SFR should then follow a relation of the type:

$$\Sigma_{\rm SFR} \propto \Sigma_{\rm gas}(P/P0)^\alpha. \tag{3.21}$$

Blitz and Rosolowsky (2006) found that their observations in 14 galaxies (including the Milky Way) were in good agreement with such a relation with an index close to $\alpha \sim 0.9$, also found in other studies (see Leroy et al. 2008, and references therein). Blitz and Rosolowsky (2006) noticed however that under their assumptions (constant velocity gas dispersion, turbulent pressure providing support), their expression is equivalent to $R_{\rm mol}$ being a function of the midplane gas density and that their data alone cannot distinguish these possibilities. They stressed that while they suggest that the hydrostatic pressure determines the molecular fraction, it does not determine how the GMC are assembled from molecular gas, or if the gas is first assembled into GMC-sized object, and then becomes molecular. In other words, even if they argue that the hydrostatic pressure plays a major role, there is room for other processes in the formation of GMCs and then, likely, of stars.

Monaco et al. (2012) found that their multiphases models including a pressure-determined molecular fraction do produce a dynamical relation ($\Sigma_{\rm SFR} \propto \Sigma_{\rm gas}\kappa$) that they interpret as resulting from the equilibrium between the energy injection (via supernovae) and dissipation.

Krumholz et al. (2009) proposed an alternate model based on the combination of few simple ideas. The Hydrogen self-shielding determines the amount of molecular gas that once formed is regulated by internal process and form stars at a rate of 1% per free fall time (as a result of turbulence). This allows them to predict the $\Sigma_\psi - \Sigma_{\rm gas}$ relationship (as well as the molecular fraction) as a function of the metallicity of the gas.

2.3.8 Influence of the Spiral Arms?

The first impression when one looks at most nearby spiral galaxy is that young stars are distributed along spiral arms or arcs, and it is hard to think that star formation is unrelated to spiral structure. Elmegreen (1979) however suggested that two types of spiral arms should be considered. The spiral density wave, related to the stellar underlying density, is responsible for the grand design spirals that are often seen in galaxies. The other type is made of stochastic spiral arms or filaments produced by the shear of self-propagating star formation (this type of stochastic arms would be a product of star formation but would not affect the galaxy SFR). According to Elmegreen (1979), the density wave/grand design arms can play an active role by compressing or shocking the interstellar material. Cowie (1981) also found that the gaseous disk of the Milky Way is globally stable against collapse, but that the passage of the clouds ensemble trough the spiral arm will modify the velocity dispersion of the clouds and produce the instability. Star formation should then proceed only in the arms. Through such processes, grand-design spiral arms should affect star formation. If star formation (or cloud collapse) is indeed enhanced when the gas crosses the arms, then the efficiency of star formation should depend on the frequency at which it happens. On this basis, Wyse (1986) proposed that

$$\Sigma_\psi \propto (\Omega - \Omega_P). \tag{3.22}$$

Ω_P is the angular velocity of the spiral pattern. This term should in fact come in combination with other factors, depending on which of the processes adopted above is considered (e.g., one of the (❯ 3.10), (❯ 3.12), (❯ 3.14), (❯ 3.15), (❯ 3.19), and (❯ 3.21)). Considering that Ω_P of the density wave is small with respect to the angular frequency of the material, the factor above becomes simply Ω. Wyse (1986) combined it with a cloud-cloud assumption to compute the SFR as $\Sigma_\psi \propto \Sigma_{HI}^2(\Omega - \Omega_P)$, and it was generalized in Wyse and Silk (1989) in $\Sigma_\psi \propto \Sigma_{HI}^n \Omega$ (n = 1,2). Interestingly, in combination with the total gas density rather than HI, the spiral arm term (❯ 3.22) suggests again a form similar to (❯ 3.17) even if it is for a totally different reason! This form seems to be robust in the sense that it accommodates various theories.

Before closing this section, it should be noted that active star formation is present even when no strong spiral structure is present (e.g., Kennicutt 1989; Tan 2000), and no clear-cut differences in star formation rates between grand-design and flocculent spirals was ever established. Maybe after all, the differences induced by the grand design spiral arms are minor, organizing the star formation in a different way rather than enhancing it.

2.3.9 Galactic Influences on the SFR: A Tentative Summary

Many theoretical ideas lead to different relations between various quantities and the SFR. The problem is that some of these ideas actually drive to the same relationships (at least under some of the possible assumptions). For instance, the dynamical factor Ω can appear as a reference to spiral arms or instabilities of the disk. Also, the ISM phase balance can under some conditions be directly related to the gas density (and thus hide in another index of a dependence on Σ_{gas}). In the case of a self-regulated star formation rate (constant Q), the same expression can be obtained based on different Q definitions (collapse versus dispersion due to Coriolis forces or shear). Moreover, the proposed explanations are not totally exclusives: the self-regulation ($Q = 1$) could be view as an approximation of the H2/HI equilibrium regulated by SN feedback!

Following the approach of Larson (1992) already mentioned, it is possible to try to write a general form for the factors affecting the star formation rate, by combining all the previously described ones. For a flat rotation curve, this general form would be (willingly forgetting other possible factors, e.g., the stellar surface density)

$$\Sigma_\psi \propto \Sigma_{\rm gas}^{\alpha} \Omega^{\beta} P^{\gamma} \tag{3.23}$$

(with α between 1 and 4, β between 0 and 2, γ between 0 and ~1). Unfortunately, these indexes are partly degenerated since, e.g., $\Sigma_{\rm gas}$ and Ω both decline with radius within galaxies. It will then be hard to derive them from observations alone.

Nevertheless, observational studies (see ❯ Sect. 4) will allow us to have a minimum of constraints on the possible relation between star formation and various quantities. This may help us to decide among the various processes at play which is the leading one (but it is already visible that this task will be hard). Even if the physical basis for these relations stay under debate, they will still provide useful constraints for models of evolution of galaxies.

2.4 Starbursts and Peculiar Star Formation Regimes

Up to this point, star formation has been discussed as a secular process occurring in a galactic disk. There are however different situations.

Starbursts regions (or galaxies) are characterized by elevated star formation rates, with an unusually high efficiency (e.g., Larson 1992, and references therein). Characterized by some signatures such as blue colors (Searle et al. 1973) and strong high-excitation emission lines, they form an ill-defined family of objects (e.g., Meurer et al. 1995, 1999) with large SFR (in absolute value, but also relative to the past average SFR, or in surface density) and short consumption timescales (the SFR is so high that the gas reservoir would be quickly depleted at this rate). As a result, the term apply to a number of objects that are not necessarily similar (especially when comparing high and low redshift ones).

Starbursts are often found in the nuclear regions of galaxies. This nuclear emission is found in an increasing fraction of galaxies with types going from early (8% in S0) to late (80% in Sc-Im) (Kennicutt 1998a, and references within). ❯ Eq. 3.15 suggests that the high level of star formation in central regions could be related to the elevated densities and high values of κ that are found there.

Starbursts are also revealed in the far infrared (FIR) with the observation of galaxies with very large luminosities (up to $10^{13} L_\odot$) corresponding to SFR up to 1,000 $M_\odot$ year^{-1}, occurring in very dense molecular gas, in which the optical radiation is almost totally absorbed. Kennicutt (1998a) reminds that the most luminous galaxies in FIR are systems in which a mass of gas corresponding to the total ISM of a normal galaxy is compressed into a small area and entirely transformed into stars.

It is tempting to relate the peculiar regime of starbursts to tidal encounters and mergers that could be responsible for enhancing the SFR by factor 10–100 (Kennicutt 1998a). Recent interactions and mergers simulations by, e.g., Di Matteo et al. (2008) produce a modest enhancement of the SFR (by a factor 5) but the modes of star formation during major mergers may need high-resolution simulations and hence be hard to catch in simulations in general (see, e.g., Teyssier et al. 2010, obtaining a gain of a factor 10 in star formation efficiency with high-resolution simulations). Barnes (2004) proposed that a shock-induced mode of star formation takes place

during such interactions. This mode is usually not taken into account (and hard to model in general) but provided a good fit to the observations of the Mice system.

3 Measuring Star Formation Rates

Before discussing the various observational evidences and especially those linked to theoretical expectations of the previous section, it should be presented how the SFR is actually measured. A famous review concerning tracers of star formation can be found in Kennicutt (1998a) whose formula are widely used. The reader is referred to this paper for many interesting discussions on the various tracers of the SFR. Recently, Calzetti et al. (2009) reviewed the subject, focusing in the long wavelength range (infrared and radio).

Almost all SFR measurements rely on few principles and assumptions. The main idea is to have an observable linked to the amount of recent star formation, i.e., of stars formed within the last time interval δt, with δt being small with respect to the age of the galaxy. Since massive stars do have short lifetimes (that can be associated to δt), astronomers can use them (or their observable effects) to derive the SFR. Once the amount of massive stars formed during δt is known, it is easy to calculate the total amount of stars formed (in solar masses) by extrapolating over the full IMF and divide by δt to get a rate (the SFR).

Often, it is not possible to actually count massive stars. Instead, some emission (that will be called a "star formation tracer") due to their presence is measured, and the actual SFR is deduced from the flux detected through calibrations described below.

A purely "instantaneous" rate cannot be measured. All tracers have different typical timescales associated, depending on the mass range of the stars they are related to. Thus, the tracers are calibrated by assuming the SFR is constant over the typical timescale δt for this tracer (e.g., the lifetimes of stars responsible for it). In other words, an assumption of steady state is made to compute the SFR. Note that the SFR deduced; in this way is well an estimate assuming that the SFR was constant over the timescale δt, and not the average of the actual SFR during this period (*Fig. 3-1* shows that the two are not equivalent).

Finally, in the following, "primary tracer" is used for measurements directly related to massive stars. The expression "secondary tracer" is used for those tracers that were introduced (at least historically) by empirically noting a correlation with a primary tracer that has been used to calibrate the secondary one. It is true that often more detailed models were constructed to recalibrate secondary tracers (at the price of more complex models), but these works were still motivated by the empirical evidence of a correlation in the first place.

3.1 Proto-Stars, Young Stars and Stellar Remnants

The Milky Way is a peculiar case in terms of SFR measurement. Most of the techniques detailed below cannot be applied, at least without some modifications. However, its SFR has been studied, mostly by using as SFR tracers the number of "young objects," as it was done by Schmidt (1959) early on. Guibert et al. (1978) provide a list of objects related to recent star formation that can be used to trace the SFR. It includes OB stars, giant HII regions, supernova remnants, and pulsars. In the recent years, the SFR in our galaxy was studied by detecting OB stars in

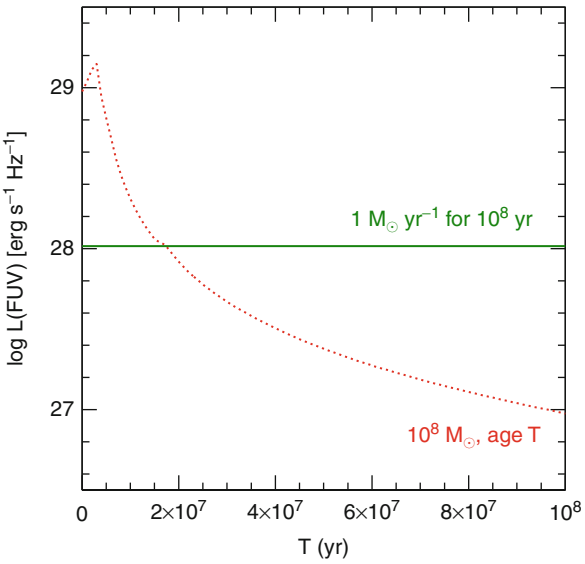

Fig. 3-1

The *dotted curve* shows the FUV luminosity (a SFR tracer) of a 10^8 $M_\odot$ instantaneous burst of age T as a function of T. The *horizontal line* shows the UV luminosity generated by a constant SFR of 1 $M_\odot$ year^{-1} during 10^8 year. All these populations have the same average SFR within 10^8 year, the timescale for the FUV emission. However, the SFR deduced from L(FUV) assuming a constant SFR can vary by 2 orders of magnitude

the far infrared. The ISM, being transparent at this wavelength, it is possible to detect star-forming regions as point-like source over the whole galaxy (e.g., Bronfman et al. 2000; Luna et al. 2006). It is also possible to detect young stellar objects (YSOs) and thus derive the SFR from pre-main-sequence objects themselves (see Robitaille and Whitney 2010).

Even if this "resolved approach" cannot be used in general for external galaxies, it is mentioned here because the spatial resolution of current and future observatories allow to contemplate the possibility to use a similar approach in our nearest neighbors (see, e.g., Whitney et al. 2008, for YSOs in the LMC).

3.2 Stellar Continuum

The continuum spectrum of a galaxy is the superposition of the emission of many generation of stars. In the UV, this emission is dominated by the hot young massive stars (above a few solar masses) and can thus be used to trace the "recent" star formation, over the lifetime of the contributing stars (of the order of 100 Myr).

For a steady state and a chosen IMF (and its mass limits), it is possible to relate the SFR and the luminosity of stars. Following Kennicutt (1998a), it can be written

$$\psi_\nu(\mathrm{M}_\odot \mathrm{year}^{-1}) = C \times L_\nu(\mathrm{ergs}^{-1}\mathrm{Hz}^{-1}). \tag{3.24}$$

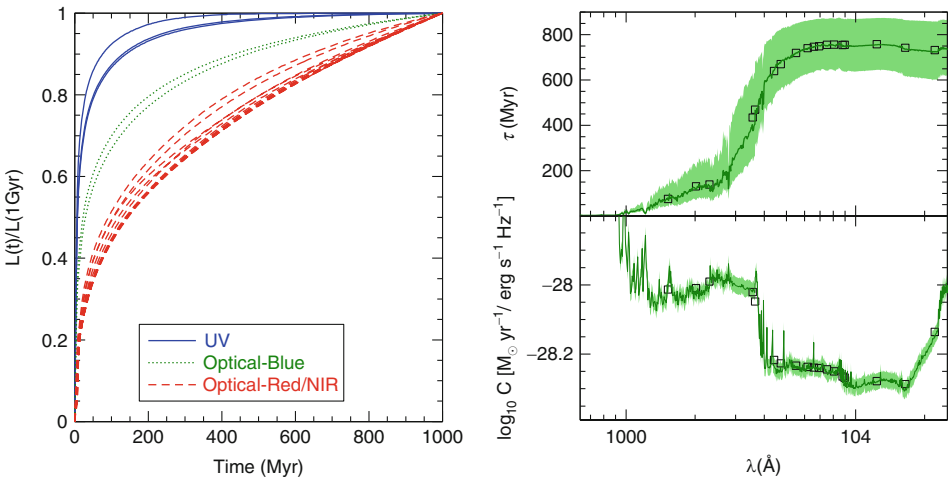

Fig. 3-2

***Left*: evolution of luminosity in a collection of photometric filters (in the UV: GALEX FUV, NUV, and FOCA; *optical/blue*: sloan u and Jonhson U; *optical/red/near infrared*: g, r, i, z, B, V, R, Rc, I, Ic, J, H, K) for a constant star formation rate of 1 $M_\odot$ year^{-1} for 10^9 years with the universal IMF of Kroupa (2001), computed using Starburst99. The luminosity is normalized by its final value. *Right-top*: time needed to reach 90% of the 1 Gyr luminosity as a function of the wavelength. (The *shaded area* shows how this curve shifts going from 85% to 95%.) *Right-bottom*: value of the calibration factor C at this time. The *squares* show the results for the same broadband filters as on the left**

The value of the conversion factor C can be computed with a spectral synthesis code, assuming a constant SFR. *Figure 3-2* shows (as a function of wavelength) the time needed for the luminosity to reach 90% of its 1 Gyr value for a constant SFR, as well as the value of C at that time. Because the SFR should be derived for massive stars with short lifetimes, this method should be used only in the UV, but the figure extends the results to the optical/near infrared for educative purpose. Short timescales are clearly obtained in the UV that makes a good tracer on ~100 Myr timescale. Fortunately, for reasonable IMFs, the L_ν luminosity per unit frequency in the UV has a relatively flat spectrum so that the calibration factor C depends weakly on the wavelength in this range. The various proposed calibrations however vary by 0.3 dex, depending on the stellar libraries used (Kennicutt 1998a). Calibration factors (and associated timescales) are provided in *Table 3-1* for several common photometric bands.

The "U" bands are intermediate: their flux to SFR conversion factor is close to the UV one, but the timescales are getting larger (about 500 Myr to the 90% level as defined previously) and thus are not as good to trace recent star formation.

3.3 Recombination Emission Lines

3.3.1 Motivation and General Approach

The strong flux emitted by young massive stars at shorter wavelengths than the Lyman limit ionizes the gas surrounding them. The recombination lines that follow can be used to estimate

Table 3-1
Primary SFR tracers. Timescales and coefficients are computed using Starburst99, solar metallicity, with the Kroupa (2001) "universal" IMF (0.1–100 $M_\odot$, slope x = 0.3/1.3 below/above 0.5 $M_\odot$). Values are given (adopting a constant SFR) when the luminosity reach 90% of the luminosity after 1 Gyr

Observation	Timescale	C	Comments
YSOs, stars, and remnants	Variable		Traditional method in the Milky Way, difficult in distant objects
		ln (➤ 3.24)	
1,524 Å(FUV-GALEX)	75 Myr	$0.97\ 10^{-28}$	Easy at high redshift, but large/uncertain extinction
2,018 Å(UV-FOCA)	131 Myr	$0.98\ 10^{-28}$	
2,308 Å(NUV-GALEX)	139 Myr	$1.02\ 10^{-28}$	
3,561 Å(u)	434 Myr	$0.95\ 10^{-28}$	Longer timescales
3,651 Å(U)	469 Myr	$0.89\ 10^{-28}$	
		ln (➤ 3.26)	
Hα	6.5 Myr	$5.1\ 10^{-42}$	Strong line, short timescale but difficulties with extinction, NII contamination, diffuse/absorbed fractions, sensitive to the upper IMF slope
Lyα	6.5 Myr		Lyα/Hα = 8.11 in theory but has to be multiplied by the unknown escape fraction

this ionizing flux and hence the SFR. The most famous SFR tracer among recombination lines is Hα (owing to its strength), but many lines from the Balmer, Pashen, and Brackett series have been used too.

For Hβ, it is possible to write (Osterbrock and Ferland 2006), assuming that all the photons are absorbed and reemitted:

$$L(H\beta) = h\nu_{H\beta} N_{\text{photons}} \frac{\alpha_{H\beta}^{\text{eff}}}{\alpha_B}, \tag{3.25}$$

where N_{photons} is the number of ionizing photons. N_{photons} can be obtained from stellar synthesis codes (such as Starburst99 for instance). For a temperature of 10,000 K and Osterbrock case B recombination, the recombination coefficients are $\alpha_{H\beta}^{\text{eff}} = 3.03\ 10^{-14}\text{cm}^3\text{s}^{-1}$, $\alpha_B = 2.59\ 10^{-13}\text{cm}^3\text{s}^{-1}$. Relations for other hydrogen recombination lines can be computed using the relative intensities of these lines with respect to $H\beta$ (Table 4.4 of Osterbrock and Ferland 2006). For instance, in the above-mentioned conditions, $L(H\alpha)/L(H\beta) = 2.847$, $L(P\alpha)/L(H\beta) = 0.332$, $L(P\beta)/L(H\beta) = 0.162$.

It is thus possible to use these relationships to compute the luminosity in any recombination line for a constant SFR and thus calibrate a relation between this luminosity and the SFR. For the same assumptions used for the stellar continuum (Kroupa 2001 IMF, constant SFR for 1 Gyr), the 90% level is reached in 6.5 Myr, almost instantaneously with respect to the long timescales obtained even with the UV continuum. This comes from the fact that the ionizing photons are on average emitted by more massive stars with shorter lifetimes than the one dominating the UV spectrum.

3.3.2 Application to Hα

Since Hα is a strong emission line with a short timescale, relatively easy to observe, moreover with good spatial resolution, it is an important tracer of star formation, and this section presents some more considerations about it. Using the method and formulae underlined in Sect. 3.3.1, it is possible to calibrate the relation between the Hα line intensity and the SFR:

$$\psi_{H\alpha}(\mathrm{M}_\odot\,\mathrm{year}^{-1}) = C \times L(H\alpha)(\mathrm{erg\,s}^{-1}). \tag{3.26}$$

The coefficient is given in *Table 3-1*, along with other SFR indicators.

Despite the advantages of Hα, making it the preferred SFR tracer, many uncertainties and difficulties exist. First, a dispersion between calibrations of 30% is due to various stellar models (e.g., Kennicutt 1998a), and the result is also very sensitive to the IMF slope in the very upper mass range. Hα, in order to be a precise tracer of the SFR must take into account the extinction that reduces the observed luminosity (see discussion on the role of dust in Sect. 3.4). When narrow-band filters around Hα are used to measure the luminosity of the line, it is also necessary to take into account the contamination of the Hα line by the neighboring [NII] λ 6548 and 6584 lines. In the absence of spectroscopy, typical ratios are used, see, e.g., the appendix of Boselli et al. (2001) for ratios given as a function of morphological type.

A fraction of the ionizing photons is in fact absorbed by dust rather than by the gas. Thus, the calibration should be corrected for this fraction that is not participating in the ionization. This fraction is estimated to be equal to 20% by Charlot et al. (2002), 0–30% by Bicker and Fritze-v. Alvensleben (2005) depending on the metallicity of the object.

Finally, a fraction of the ionizing photons may escape the HII regions. While in individual regions this escape fraction can be high (15–50%), it is thought to be lower on the scale of galaxies as a whole (Kennicutt 1998a, and references therein).

3.3.3 Lyman α

From the above, it is easy to find that the Lyα luminosity should be large, and thus should be a good tracer of star formation. This emission line has in fact been used in the recent years to search and find high redshift star-forming galaxies. The relations Lyα/Hβ = 23.1 and Lyα/Hα = 8.11 are obtained for a 10,000 K case B scenario (Osterbrock and Ferland 2006) and combined with, e.g., (3.26) should allow us to derive the SFR from the Lyα luminosity. It is however a poor SFR tracer, and measurements are systematically lower than these predictions.

The path length of Lyα photons in the ISM is extremely large due to resonant scattering by hydrogen atoms. Thus, they have increased chances to be absorbed by even a modest amount of dust. As a result, the resultant Lyα emission is quickly decoupled from star formation (Giavalisco et al. 1996). A Lyα escape fraction f (fraction escaping the galaxy and measurable by observers) can be defined by comparing the ratio of Lyα to other SFR tracers (Hα, Hβ, UV). Following such methods, $f \sim 0.1$ is found in the nearby universe and at redshift ~0.3 (Deharveng et al. 2008). The escape fraction seems to increase with redshift, with values of $f \sim 0.2$–0.3 around redshift 2–3, and $f \sim 1$ at very large redshifts (Gronwall et al. 2007; Cassata et al. 2011).

This evolution, statistical in nature, may tell us about the evolution of the dust and of the ISM properties with redshift but still relies on few samples. These results are based on other tracers

to measure the actual SFR, and the escape fraction is deduced by comparison. As a conclusion, Lyα is more a tool (to study the statistical properties of the ISM or to detect objects) than a quantitative SFR tracer.

3.4 The Role of Dust

The primary SFR tracers (recombination lines, UV emission) are based on luminosities which are (in most cases) sensitive to the attenuation of light by interstellar dust. The energy "lost" in the UV star light is found again in the mid and far infrared where the emission of the dust grains can be measured. In this section, corrections of primary tracers for the effect of dust attenuation are discussed, as well as the use of the dust emission itself as a SFR tracer.

3.4.1 Extinction Corrections from Recombination Lines

For Hα (or other recombination lines), corrections are usually estimated from line ratios. Observed line ratios are compared to the predictions of case B recombination, and the difference is ascribed to the differential extinction between the two wavelengths. Combined with an extinction curve, it is then possible to estimate the amount of attenuation of, e.g., Hα: A(Hα). Typical attenuations are found between 0 and 2 mag (e.g., Kennicutt 1998a). Another method consists in using the thermal radio to Hα ratio (e.g., Bell 2003).

In most cases, the Balmer ratio is used, for which Hα/Hβ = 2.847 in the T = 10,000 K case B. This view is however challenged by the models of Charlot and Longhetti (2001). When such models are used to simultaneously fit extinction and various line intensities, a dependence on the metallicity of the intrinsic Hα/Hβ ratio is found, which affects the derived extinctions (Brinchmann et al. 2004; Gilbank et al. 2010). This dependence is due to the fact that metallicity affects the cooling and thus the electron temperature of the HII regions. The typical value of 2.847 is given for T = 10,000 K, but the ratio does depend on the temperature (Osterbrock and Ferland 2006).

Observational uncertainties also affect the Hα/Hβ ratio, especially if narrow-band imaging has been used to obtain the data. As mentioned in the Sect. 3.3.2, the Hα has to be corrected for the neighboring [NII] lines. Also, the Balmer absorption features in the underlying stellar spectra have to be corrected for. In the absence of good spectroscopic data allowing to measure it, a standard absorption of 2–5 Å in equivalent width is often used (e.g., Boselli et al. 2001).

3.4.2 Extinction Corrections in the UV

The UV attenuation can be large (reaching over 4 mag). The energy lost by the absorption of UV (and optical) photons is reemitted in the mid and far infrared (between 8 and 1,000 μm). Usually, the total luminosity emited in this range is estimated on the basis of a few available bands (e.g., the IRAS 60 and 100 μm in the past, the Spitzer and Herschel bands in the more modern time). Here, this total infrared luminosity is generically called L(FIR) although different definitions (extrapolating to different infrared wavelength range and using different observations) exist (e.g., Boquien et al. 2010b, and references therein).

Because of this balance of energy, the UV attenuation is related to the $L(\mathrm{FIR})/L(\mathrm{UV})$ ratio. UV-derived star formation rates can be corrected using this ratio (Cortese et al. 2008). A limitation of the method is that at low SFR, part of the FIR emission can come from the heating by old stars, leading to an overestimate of the extinction (e.g., Iglesias-Páramo et al. 2006). Cortese et al. (2008) proposed a method correcting for this effect by using various color indexes to trace the balance between old and young stars.

In many cases, it is difficult to have far infrared data, especially at high redshift. A popular method (although uncertain) in that case consists in using the slope of the spectrum in the UV (β), which is empirically related to the $L(\mathrm{FIR})/L(\mathrm{UV})$ ratio (in the absence of dust, the UV slope is flat, the observed slope, by comparison, can be ascribed to dust). The method is however known to suffer some problems. For instance, different attenuation curves may affect the shape of the spectrum, independently of the amount of dust itself. And mostly, it was shown that local normal galaxies and starbursts provide quite different relations between β and the UV attenuation (Buat et al. 2010; Muñoz-Mateos et al. 2009; Seibert et al. 2005; Kong et al. 2004; Meurer et al. 1999).

3.4.3 Other Considerations on the Dust Attenuation

In the absence of a better indication, "standard" extinctions are sometimes applied to large samples. However, the extinction may depend on the SFR itself (Hopkins et al. 2001; Bell 2003) or on other properties such as the galactic mass or metallicity. While the trends in the nearby universe are relatively well studied, such relationships at high redshift are very uncertain, mostly in reason of the very different selection criteria of various samples (e.g., Gilbank et al. 2010). It is believed that moving toward higher redshift, the extinction increases (as the cosmic SFR does). Eventually, the extinction should decline again when a metal-poor era is reached, and there is some claim of indirect measurements of this effect in the recent high-redshift studies (e.g., Cucciati et al. 2012). The question of the cosmic evolution of dust extinction is however still open and debated.

Another point to note is that extinction corrections are more difficult to apply on small spatial scales than on the global scales of galaxies. For instance, in the case of the UV attenuation estimated from the far-infrared radiation, the heating of a small region can come from UV photons emitted in a neighboring region rather than from the one studied.

The UV emission coming from older stars than the Hα emission, the position of the various type of stars may be decoupled, and their distribution with respect to dust different. In that case, attenuation derived for a population may not apply to another one. In fact, it is thought that the nebular lines are attenuated by roughly twice as much dust as the stellar continuum (because young stars are found inside dust-rich molecular clouds, while the old stellar population has drifted away from the dusty regions (Bell 2003; Calzetti et al. 1994) or because the dust clouds have themselves a finite lifetime (Charlot and Fall 2000). In her "recipe for reddening," Calzetti (1997) suggests that the reddening of the stellar continuum is 0.44× the reddening in the Balmer lines.

3.4.4 Far-Infrared Star Formation Rates

Since a large amount of the stellar emission in the UV is absorbed by dust and the energy is radiated in the far infrared, this dust emission itself can be used as a SFR tracer.

Table 3-2

Secondary far-infrared SFR tracers. The timescale is about the one for the production of UV photons since they dominate the heating of the dust. It however depends on the star formation history because of the contribution to the dust heating by older stars. Calibrations published by various authors using the same IMF as in the primary tracer table are provided. These tracers were calibrated on primary tracers corrected for extinction, mixed tracers, or on models including absorption and emission by dust

Tracer	$\psi(M_\odot\ year^{-1})$ =	Comments
FIR	$1.07\,10^{-10}(L(FIR)/L_\odot)$	Assuming total opacity in the UV (Buat et al. 2008), that works well for high SFRs. Limits: contribution to the heating by old stars, not taking into account the part of the SFR not extinguished
24 μm	$2.50\,10^{-43}(L(24)/erg\,s{-}1)$	Calzetti et al. (2010) and references therein.
70 μm	$5.88\,10^{-44}(L(70)/erg\,s^{-1})$	Calzetti et al. (2010)
160 μm	$1.43\,10^{-43}(L(160)/erg\,s^{-1})$	This is not a proper calibration because of the large dispersion and the dust heating by old stars according to Calzetti et al. (2010)
250 μm	$8.71\,10^{-45}(L(250)/erg\,s^{-1})^{1.03}$	From Verley et al. (2010b) but only calibrated in HII regions of M33. Same difficulties as above

Buat and Xu (1996) found that galaxies follow a relation of the type $L(\mathrm{FIR}) = 1,680\,\text{Å} \times L(2,000\,\text{Å})$ where L(2,000 Å) is the UV luminosity, corrected for extinction, and L(FIR) is an estimate of the total luminosity emitted in the FIR range. Combining such a relation to a calibration between the UV emission and the SFR, one can calibrate a relation between the SFR and the FIR emission (Buat and Xu 1996; Kennicutt 1998a) (*Table 3-2*). This relation is however dispersed by a factor 3 (Buat and Xu 1996), and the method should be valid in galaxies with high star formation rates where dust is mostly heated by young stars, with a negligible contribution by older stars.

Under the assumption that the ISM is totally opaque, the whole luminosity emitted by the stars should be found in the infrared. It is then possible to compute the infrared luminosity L(FIR) for a constant SFR. Buat et al. (2008) proposed for the same IMF adopted above:

$$\log(\psi[M_\odot\ year^{-1}]) = \log(L(FIR)[L_\odot]) - 9.97. \tag{3.27}$$

This relation cannot be applied blindly to, e.g., dwarf galaxies and system with low SFRs that are usually suffering low extinctions and in systems with low activity in which the dust is heated by lower mass stars, with longer timescales (but, e.g., Bell 2003, proposed a calibration taking into account this effect.)

Instead of using the total far-infrared emission as above, some authors have argued that it is best to use monochromatic far-infrared indicators. The main reason is that it avoids the need to extrapolate from few measured points to compute the total luminosity and that some wavelengths may be associated in a closer way to the hot dust directly tracing star formation. Calzetti et al. (2009) reviewed many calibrations proposed for the Spitzer telescope observations at 24 μm and proposed relationships for the monochromatic luminosities at 70 and 160 μm. The 8 μm emission was also studied but this wavelength is a poor tracer of star formation (Calzetti et al. 2007). Boquien et al. (2010a) provided a SFR surface density–surface brightness calibration for the Herschel PACS bands at 100 and 160 μm on the basis of Herschel observations of M33.

Herschel SPIRE 250 μm observations of M33 were used by Verley et al. (2010b) to provide a calibration of the SFR from 250 μm.

3.4.5 The Mixed Tracers

Finally, it was recently proposed a family of "mixed" tracers, combining optical or UV, and infrared observables.

As mentioned above, the SFR deduced from the infrared is either empirically derived or is derived under the assumption of full transfer of the energy from the UV to the infrared. For galaxies of low masses, this assumption is usually wrong. It has been proposed to compute the SFR in a more general situation by combining an infrared tracer (that gives us the amount of energy transferred to the infrared by dust), and an optical/UV tracer (that gives us the amount of young stars whose light is not extinguished by dust. Iglesias-Páramo et al. (2006) proposed such a mixed tracer:

$$\psi = \psi_{\mathrm{UV,obs}} + (1-\eta)\psi_{\mathrm{dust}}. \tag{3.28}$$

The first term is the SFR derived from the observed UV luminosity (following (3.24)), the second term is the SFR traced by dust (3.27). η accounts for the IR cirrus emission: this diffuse component of dust heated by the interstellar radiation field generated by old stars, and not directly tracing the SFR. The value of η depends on the samples under study. From 0 for starbursts, it can reach 0.4 for star-forming galaxies (Iglesias-Páramo et al. 2006; Hirashita et al. 2003; Bell 2003).

Kennicutt et al. (2009) proposed several calibrations of mixed tracers composed of Hα (or [OII]) lines and IR (or radio) tracers. They take the form:

$$\psi = C(L(\mathrm{line,observed}) + a\,L(\mathrm{dust})). \tag{3.29}$$

C is the calibration factor that relates directly the luminosity in a line and the SFR. $L(\mathrm{dust})$ is the luminosity in a tracer sensible to the dust-extinguished SFR. Kennicutt et al. (2009) provided values of a when 8 and 24 μm, total infrared, or 1.4 GHz luminosities are used. These values are determined by fitting the coefficients using as a reference the SFR deduced from the Hα line corrected for extinction using recombination lines ratio. Expressed under the form of (3.29), the $a\,L(\mathrm{dust})$ term is nothing else than a statistical extinction correction. In order to study the spatial distribution of star formation within nearby galaxies, Bigiel et al. (2008) defined a mixed tracer by a combination of 24 μm (from Spitzer) and UV (from GALEX) luminosities since these two wavelength are observed with a similar resolution.

A nonexhaustive list of mixed tracers that have been proposed in the literature can be found in *Table 3-3*.

3.5 Other Spectral Diagnostics

3.5.1 [OII] 3,727 Å Forbidden Line

Especially at high redshift, the oxygen emission doublet [OII]λ3727 is often used because of its strength to detect galaxies and attempt to measure their SFR. Such forbidden lines are however not as directly related to the stellar emission as the primary tracers. The line luminosity

Table 3-3
Mixed tracers. They are in general calibrated on extinction-corrected primary tracers

ψ =	Interest and difficulties
$\psi_{UV,obs} + (1-\eta)\psi_{dust}$	η depends on the sample (Iglesias-Páramo et al. 2006).
C(L(line, observed) + a L(dust))	a L(dust) is a statistical extinction correction, calibrated for 8, 24 μm, total infrared, and 1.4 GHz. Coefficients are given in Kennicutt et al. (2009) for the Hα and [OII] lines.
$0.68\,10^{-28}$L(FUV) + $2.14\,10^{-42}$L(24 μm)	Appendix D of Leroy et al. (2008)

is much more sensitive to temperature and ionization state of the gas than recombination lines such as the Balmer lines. The [OII] line has been calibrated empirically by noticing that a good correlation exist anyway between the [OII] and Balmer lines luminosity. Gallagher et al. (1989) found in nearby normal galaxies $L([OII]) = 3.2L(H\beta)$ with however a factor 3 scatter at a given Hβ flux. Kennicutt (1998a) also mentions a large scatter (up to 1 dex) for the [OII]/Hα ratio.

A proper calibration has to take into account the respective extinction in the two lines. Kewley et al. (2004) found an average ratio of [OII]/Hα = 1.2 ± 0.3 that can be combined with a Hα-calibrated SFR to compute the SFR. However, this oxygen line is clearly affected by metallicity (see Sect. 3.8.1).

3.5.2 [CII] 158 μm Fine structure line

The [CII] 158 μm line is the more important coolant of the warm neutral interstellar medium, while the heating of the gas is related to the incident FUV emission (Malhotra et al. 2001, and references therein). It is thus linked to star formation in an indirect way. Malhotra et al. (2001) presented a statistical comparison of the line emission with the far-infrared one: the ratio $L([CII])/L(FIR)$ has a value about $3\,10^{-3}$ with a large dispersion (factor 50). They also found a trend with the temperature of the dust, indicated by the ratio of the luminosities at 60 and 100 μm. Within M31, Rodriguez-Fernandez et al. (2006) showed that the [CII] line traces the regions of star formation, identified with Hα or at 24 μm.

While opening a possible large area of interest for the future, this line is not yet a popular tracer of star formation.

3.6 Radio Emission

The radio emission in normal galaxies come from synchrotron radiation from relativistic electrons and free-free emission from HII regions (see the review of Condon 1992, for all this section). The relativistic electrons are thought to have their sources in the supernovae remnants (SNRs) appearing in galaxies after the explosions of massive stars. The radio emission is thus associated to short-lived massive stars. Since the FIR emission is also linked to star formation (see Sect. 3.4.4), a relation between the radio emission and the FIR emission should be

observed, and it is indeed the case in nearby galaxies The FIR-radio correlation can be expressed as (Condon 1992, and references therein)

$$\log(S_\nu) = \log(\mathrm{FIR}) - q. \tag{3.30}$$

q is observed to have a median value of 2.3 at 1.4 GHz (even if the relation is not perfectly linear, especially at low luminosity where the radio emission is lower than predicted by this equation). Though this relation, the radio emission can be considered as a secondary tracer of star formation. Simple models allow to reproduce this relation between SFR, FIR, and radio emission, although the physics is not clearly understood (see Condon 1992, for a much longer discussion). Bell (2003) noted that both the FIR and radio emission underestimate the SFR at low luminosities and proposed a calibration taking this effect into account.

Because the electrons travel in the galaxy before emitting their radiation, this indicator may not bring spatial information on very small scales. Murgia et al. (2002) however suggests that the Hα and radio continuum trace each other well even on scales of a few kpc.

3.7 X-Ray Luminosity

Star-forming galaxies host a number of sources of X-ray emission: high mass X-ray binaries, supernovae remnants and hot plasma (Ranalli et al. 2003). Observations show that the X-ray luminosity (Ranalli et al. 2003) and the number of high mass X-ray binaries (Grimm et al. 2003) correlate with other SFR tracers, what allows to derive the SFR from the X-ray luminosity. The relations provided by Grimm et al. (2003) are included in *Table 3-4*. The dispersion obtained in the various relations is typically 0.25–0.3 dex. It is also possible to develop more complex models linking this secondary indicator to the SFR (Grimm et al. 2003).

Table 3-4

Multiwavelength secondary SFR tracers. The relations with other tracers are provided instead of actual SFR calibrations (that can be obtained by combining these relationships with the adequate calibration)

Tracer	Calibration	Comments
[OII]	$[\mathrm{OII}]/\mathrm{H}\alpha = 1.2$	Strong at high redshift. Limits: extinction, dependence on ionization state and metallicity.
[CII] 158 μm	$\mathrm{L}([\mathrm{CII}])/\mathrm{L}(\mathrm{FIR}) \sim 3\,10^{-3}$	Large scatter, dependence on dust temperature (Malhotra et al. 2001)
Radio emission	$\log\left(\frac{S_{1.4\,\mathrm{GHz}}}{\mathrm{Wm^{-2}Hz^{-1}}}\right) = \log\left(\frac{\mathrm{L(FIR)}}{3.75\,10^{12}\,\mathrm{Wm^{-2}}}\right) - 2.3$	From Condon (1992). Not affected by extinction. Possible loss of the spatial information
Soft X-ray Hard X-ray	$\log\left(\frac{\mathrm{L(0.5-2\,keV)}}{\mathrm{erg\,s^{-1}}}\right) = \log\left(\frac{\mathrm{FIR}}{\mathrm{erg\,s^{-1}}}\right) - 3.68$ $\log\left(\frac{\mathrm{L(0.5-2\,keV)}}{\mathrm{erg\,s^{-1}}}\right) = \log\left(\frac{S_{1.4\,\mathrm{GHz}}}{\mathrm{erg\,s^{-1}\,Hz^{-1}}}\right) + 11.08$ $\log\left(\frac{\mathrm{L(2-10\,keV)}}{\mathrm{erg\,s^{-1}}}\right) = \log\left(\frac{\mathrm{FIR}}{\mathrm{erg\,s^{-1}}}\right) - 3.62$ $\log\left(\frac{\mathrm{L(2-10\,keV)}}{\mathrm{erg\,s^{-1}}}\right) = \log\left(\frac{S_{1.4\,\mathrm{GHz}}}{\mathrm{erg\,s^{-1}\,Hz^{-1}}}\right) + 11.13$	Ranalli et al. (2003). This tracer has the advantage of not suffering extinction, but the calibrations are dispersed

3.8 Additional Factors

All the tracers have been discussed above adopting an IMF and assuming a solar metallicity. Adopting other assumptions could change the calibrations of the SFR tracers easily by a factor up to 2 (see below), even for the primary tracers. Another difficulty is the steady-state assumption that may not always hold. These aspects are discussed in the rest of the section.

3.8.1 The Effect of the Metallicity

The primary tracers of the SFR depend on the metallicity as low-metallicity stars have higher temperatures, higher UV luminosities and ionizing fluxes. Bicker and Fritze-v. Alvensleben (2005) calibrated the dependence on the metallicity of the C factors in (3.24) and (3.26). Both calibration factors vary with the metallicity by a factor about 2 between low and high metallicity. The reader is refereed to Bicker and Fritze-v. Alvensleben (2005) for quantitative values.

The [OII] line emission can also be computed through detailed modeling, and Bicker and Fritze-v. Alvensleben (2005) provide also a calibration of its dependence on metallicity. The influence of metallicity on the luminosity of this line was also investigated by empirical studies that established that the [OII]/Hα ratio does vary with metallicity. This dependence was calibrated by Kewley et al. (2004). Mouhcine et al. (2005) however showed that even this calibration does not catch all the physics at play. They found a non-monotonic relation between the [OII]/Hα ratio and the metallicity. They also found that, in addition, the ionization state affects the ratio, especially in metal-poor active starbursts.

Technically, all the secondary tracers calibrated on one of the primary tracers (with an explicit dependence on metallicity) should present the same dependence on metallicity.

3.8.2 Choice of the IMF

Since the primary tracers are related to the more massive stars, but the SFR is integrated over the whole IMF, the calibration factors are very sensitive to the form of the IMF (that determines how many massive stars are present per unit stellar mass formed). A proper computation is necessary to provide a calibration. *Table 3-5* quotes a few transformation formulas that can be found in the literature and provides an idea of the uncertainty due to the IMF. Seeing these

Table 3-5
Effects of the choice of the IMF on the SFR calibrations. This nonexhaustive list of values is collected from the literature (they are not 100% consistent with each other)

Conversion	Reference
ψ(Kroupa 2001) × 1.5 = ψ(Salpeter)	Brinchmann et al. (2004)
ψ(Kroupa 2001) × 1.59 = ψ(truncated Salpeter)	Bigiel et al. (2008)
ψ(Chabrier 2003) × 1.5 = ψ(Salpeter)	Schiminovich et al. (2010)
ψ(Kroupa 2001) × 1.5 = ψ(Salpeter)	Argence and Lamareille (2009)
ψ(Kroupa 2001) × 0.88 = ψ(Chabrier 2003)	Argence and Lamareille (2009)

numbers, it is obvious that the choice of the IMF can affect the SFR by a factor at least as large as the metallicity influence or the fraction of Lyman continuum photons not contributing to the ionization of the gas.

There is good reason to think that the IMF is universal (Bastian et al. 2010). In that case, such a global correction should allow us to switch from one IMF to another. However, the idea of variations of the IMF come back to haunt extragalactic astronomers frequently. GALEX allowed discovery of a surprisingly high fraction of galaxies with extended UV emission, interpreted as extended star formation (see Sect. 4.3). This discovery, together with the fact that Hα (very sensible on the IMF slope at high masses) had not revealed this star formation, previously led to some speculations about the possible variation of the IMF with radius within galaxies, probably through a physical dependence on other quantity, such as the gas density or the total SFR. Krumholz and McKee (2008) proposed a gas density threshold for the formation of massive stars, while Pflamm-Altenburg et al. (2007) suggested that the IMF for a whole galaxy (what they call the integrated galactic initial mass function, IGIMF) results from the combination of the cluster mass distribution and the IMF within clusters. In their approach, the maximum stellar mass in a star cluster is limited by the cluster mass, and the maximum cluster mass depends on the SFR. As a result, they found that the IGIMF does depend on the SFR. If confirmed, such a variation would have important consequences, the first one being that the calibrations discussed above would be false, especially at low SFRs.

This motivated several studies on measurements of the Hα/UV ratio in small galaxies and outer parts of spirals and its interpretation, with conflicting results. In addition to the difficulty due to measurements and calibrations, the situation is complicated by the fact that this ratio may also depend on other factors (e.g., different attenuations, variation of the fraction of ionizing photons absorbed by the dust, micro-history of the star formation: see next section). As a result, a clear situation has not emerged yet, but several works are ongoing on the subject.

A variation of the IMF with the redshift has also been advocated (with a top-heavy IMF at high redshift), for instance, to reconcile the evolution of the SFR and stellar mass cosmic average densities (e.g., Wilkins et al. 2008a).

In summary, suggestions of IMF variations are proposed in various contexts, and their possibility should be kept in mind. However, the subject stays under debate because of the complexity of the observations and the possible alternate explanations.

3.8.3 Effect of the Star Formation Micro-History

The steady state assumption was applied to calibrate the relationships between star formation tracers and SFR described before. This seems to be a reasonable assumption when considering normal galaxies as a whole. However, it cannot be applied to, e.g., very small individual regions inside galaxies (e.g., individual star clusters). A minimum scale is needed to average out the stochasticity of star formation. The assumption may also break down for starbursts (or post-starbursts), in which the star formation history is undergoing (or has undergone) large and sudden variations, or in small galaxies, where for stochastic reasons the micro-history of star formation (over the last 10–100 Myr) may present significant variations. When there is reason to believe that the star formation history was not constant over δt, time corresponding to the timescale of the tracer used, a meaningful SFR cannot be derived with this tracer. It is still possible to study these objects, but it is then necessary to obtain data constraining, e.g., the total mass that was formed during a star-forming event together with the age and duration of this event.

Using resolved stars, McQuinn et al. (2010, and references therein) found that the duration of starbursts in nearby dwarf galaxies is several 100 Myr (longer than many other estimations of a starburst duration), allowing to derive reasonable SFR for tracers with similar timescales (e.g., UV). But they also found that Hα measurements sometimes provide a different result because the SFR fluctuates on a few Myr timescale. Boissier et al. (2008) also suggested that the colors of their LSB galaxies may be due to a succession of active star formation and quiescent phases.

The effect of such bursts and micro-star formation history on SFR tracers (and their ratio, especially Hα/UV) has been much discussed in, e.g., Weilbacher and Fritze-v. Alvensleben (2001), Iglesias-Páramo et al. (2004), Boquien et al. (2007), and Boselli et al. (2009). It is however difficult to disentangle from other possible effects, e.g., the IMF variations discussed in the previous section.

4 Star Formation Observed in Galaxies

Provided the assumption and limitations discussed in ❯ Sect. 3, it is possible to compare the SFR actually observed to the theoretical ideas presented in ❯ Sect. 2 and more generally discuss some empirical properties of star formation on galactic scales.

4.1 Star Formation in the Local Galaxies

Surveys of the local volume show that star formation in galaxies depends on their luminosity, gaseous content, or morphological type. This can be seen in ❯ *Fig. 3-3* reproduced from Karachentsev and Kaisin (2010) who combined Hα observations from galaxies within 8 Mpc (in addition, the overplotted open square indicates typical values for the Milky Way). The SFR is also found to depend on other quantities, such as colors (as more luminous galaxies are also redder). Another Hα survey of the local 11 Mpc can be found in Kennicutt et al. (2008). A similar study based on the ultraviolet tracer of star formation (instead of Hα) can be found in Lee et al. (2009). Some differences between Hα and UV are found especially in the smallest galaxies; see ❯ Sect. 3.8.2 for a possible interpretation. Many other surveys in, e.g., *H*α, UV, and FIR provide different views according to their selection criteria (as discussed in the review of Kennicutt 1998a).

The SFR range from ~0 in early type galaxies to a few $M_\odot$ year^{-1} in the Milky Way and relatively normal disk galaxies. However, much higher values of the SFR (up to several 100 $M_\odot$ year^{-1}) are also found in rarer starbursts (absent in the small local volume), usually associated with signs of interaction or mergers.

4.2 The Schmidt Laws

4.2.1 Preliminary Considerations: Many "Laws"

An important part of the study of star formation on the scales of galaxies revolves around the so called Schmidt Law. Although now largely in usage, the term "law" is not really appropriate as

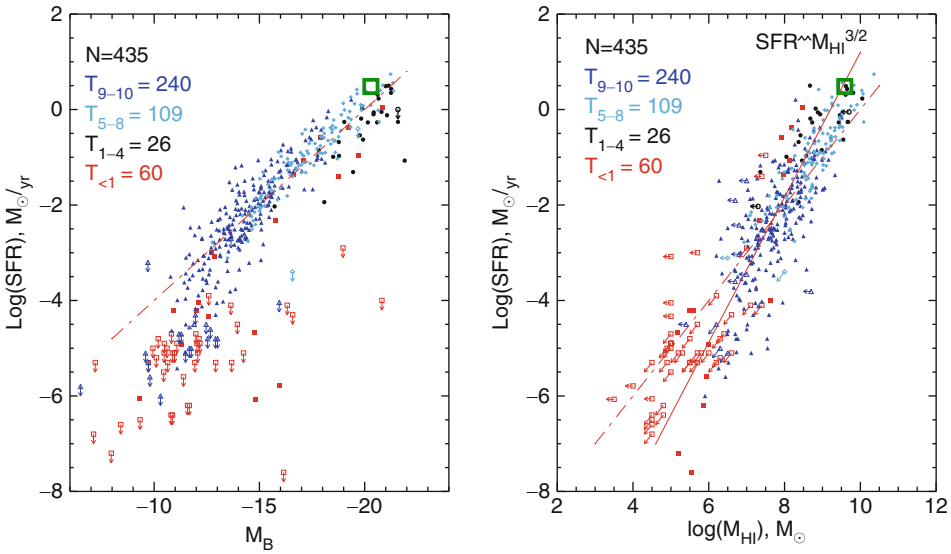

Fig. 3-3

Reproduced by permission of the AAS from Karachentsev and Kaisin (2010): Hα derived SFR in the Local Volume as a function of the B magnitude (*left*) and HI mass (*right*). The *dashed lines* correspond to a constant ratio between y- and x-axis . The *open square* indicates values typical for our Milky Way (e.g., Boissier and Prantzos 1999; van den Bergh 1999, and references therein)

it is really an empirical relationship, originally established between the number of young stars in the Milky Way and the gas volume density by Schmidt (1959). This law can be writen in this form:

$$\rho_\psi \propto \rho_{\rm gas}^n. \tag{3.31}$$

A lot of relations similar to (3.31) are called "Schmidt Laws." The first variation is the use of surface densities rather than volume densities, suggested by Sanduleak (1969) in his study of the Schmidt Law in the Small Magellanic Cloud, a form that is very frequently used:

$$\Sigma_\psi \propto \Sigma_{\rm gas}^n. \tag{3.32}$$

This form has the advantage to be more easy to reach from observations (no need to know the scale heights of disks). For a constant scale height, the index n of the volume law (3.31) is obviously the same as the one of the surface densities law (3.32). Surface densities also appear in many of the equations of Sect. 2, suggested by various theories. Indeed, surface densities in a rotating disk do play a physical role. Such a local relation between surface densities of star formation rate and gas is called "Schmidt-Sanduleak Law" by Madore (2010).

Madore et al. (1974) noticed that the index of the Schmidt Law was different in the inner and outer parts of M33, suggesting that the star formation law may change with radius within galaxies. Later, the "radial" Schmidt Law was studied on the basis of azimuthally averaged profiles (Kennicutt 1989; Kennicutt 1998b; Wong and Blitz 2002; Boissier et al. 2003, 2007).

Finally, the Schmidt Law was also studied on the scale of whole galaxies, for instance, by computing average surface densities of gas and SFR, as it is done in the seminal paper of Kennicutt (1998b). Sometimes, the total SFR and total gas amount are directly compared one to another (without normalization per, e.g., size). Following again Madore (2010), such a global law (normalized or not) can be called a "Schmidt-Kennicutt Law."

Very often, these various types of laws are compared one to another or plotted together even if this should be done only with a lot of caution. For instance, if star formation follows a local Schmidt Law, with a local critical density threshold, an analysis of the radial Schmidt Law may provide a steeper slope, and the threshold may be hard to recover (see *Fig. 3-4*). Similar differences will exist between the local Schmidt Law and a measurement of the Schmidt-Kennicutt Global Law (*Fig. 3-5*). The illustrations of these differences (*Figs. 3-4* and *3-5*) are qualitative, but based on actual simple toy models. Leroy et al. (2008) proceeded to a similar exercise: they implemented a pixel-by-pixel threshold in their data. When computing radially averaged profiles, they found that the threshold damps the average SFR but does not bring it to 0. Kennicutt (1989) had already noticed that the globally averaged star formation rate is more strongly coupled to the HI density than the radial profile, illustrating again that the various

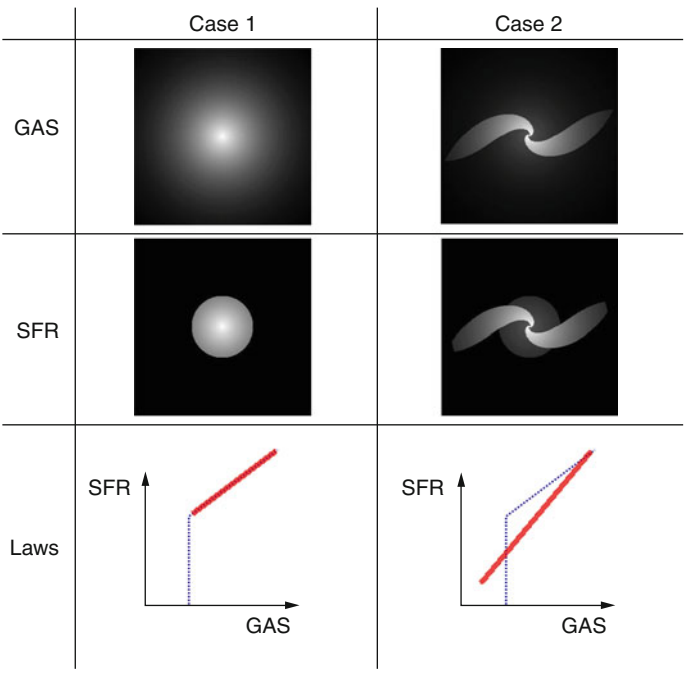

Fig. 3-4

This sketch illustrates the possible difference between a local law (*dotted blue*) and an azimuthal law (*solid red*). In case 1, the disk is purely exponential and there is no difference between the local and azimuthal laws. In case 2, two spiral arms enhance locally the density by a factor 3. While this toy model implement the exact same local law as the previous one, its slope and threshold are not recovered in an azimuthal analysis. The differences between the local and azimuthal laws are sensitive to the covering fraction of the arms and its variation with radius

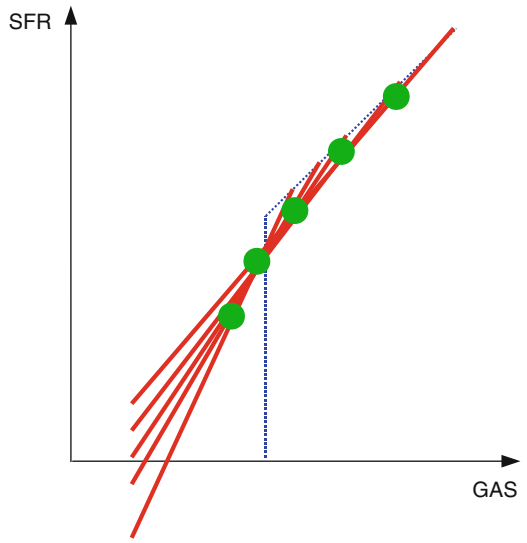

Fig. 3-5
In this illustration, several toy models were constructed with the same local law (*thin blue dotted line*). They each follow different azimuthal laws (*thick solid lines*) depending on, e.g., the radial variation of the spiral arms covering fractions. The *green points* show the global Schmidt-Kennicutt Law. Local, azimuthal, and global relationships have different slopes and do not show the same threshold

scales follow intrinsically different laws. These variations may partly explain the large range of values found in the literature for the index n (0–4), although part of this scatter traces actual differences (Kennicutt 1998a) and the limitations of a simple Schmidt Law parametrization (Kennicutt 1997), in addition to the various SFR tracers used.

These variations (local, azimuthal, global) are not the only one. The results may also depend on the SFR tracer used (see Sect. 3), but also on the gas phase used. "Gas" refer in this chapter to the total gas, but often only the neutral (mostly *HI*) or molecular (mostly H_2) is used[2] (sometimes for observational reasons, sometimes because one wants to study a process specific to one phase). In most cases, H2 is actually not observable, and other molecules are used to trace it. The most famous one is CO, but the $X_{\rm CO}$ conversion factor carries large uncertainties (see discussion in Calzetti and Kennicutt 2009). While some authors use a metallicity dependence, other prefer to keep a constant value, what may directly affect the slope of the Schmidt Law.

Table 3-6 attempts to summarize the various type of laws and the phenomenon that they probe.

Finally, the Schmidt Laws have been extended to include other factors than the gas density, especially to test the various theoretical expectations discussed in Sect. 2 (for instance, 3.23). This was motivated by the theoretical expectations, but also by the fact that a perfect fit cannot

[2]To account for the abundance of the other elements (mostly Helium), a corrective factor ~1.36 is sometimes used to go from *HI* to neutral and from H_2 to the molecular contents. On the other hand, some authors call "total gas" the sum of the *HI* and H_2 masses, i.e., the total mass of hydrogen, not including this factor.

Table 3-6
Proposed relevance of the various Schmidt Laws. Secondary factors not included!

	Local Schmidt-Sanduleak	Azimuthal Radial Schmidt Law	Global Schmidt-Kennicutt
HI	Local effects on HI/H2 phases transition	Processes affecting the formation of molecular gas on orbital timescales (e.g., spiral arms)	Transformation of the global reservoir of HI into H2
Total	Local gravitational effects	Gravitational processes occurring on orbital timescales (e.g., role of Ω)	Role of the global reservoir of gas
H2	Formation of stars in GMCs		

be obtained with a pure dependence on the gas density. First, the observed simple Schmidt Law presents a large scatter, believed to be larger than the observational uncertainties (e.g., Kennicutt 1998b). Second, it was noticed in many occasions that the Milky Way and a number of other nearby galaxies present flat HI profiles, dominating the total gas at large radii, while their SFR clearly decreases with radius. A pure dependence on the total or HI surface density alone (at least in azimuthal profiles) cannot work (e.g., Blitz and Rosolowsky 2006; Boissier and Prantzos 1999; Ferguson et al. 1998; Kennicutt 1989).

4.2.2 Which Law Is Right?

Which of the Schmidt Laws described in Sect. 4.2.1 should be used to, e.g., constrain our models ? It actually depends on the precise goal that is aimed at. To understand the very physics of star formation (how gas is turned into stars), local studies are of prime importance (the issue on which scale "local" studies should be performed is discussed below). If one wants to constrain a 2D model of galaxies, then again the local law brings more constraints.

However, it is well known that some properties depend mostly on the galactocentric radius R (e.g., the fact that star-forming galaxies display an exponential disk, the abundance, and color gradient). This is related to the fact that these quantities results from processes occurring on timescales longer than the rotation time around the center of the galaxy. 1D models (depending only on radius) are thus performed, especially in studies of chemical evolution. Such models aim at reproducing the radially averaged SF law (that tells us about how star formation is related to the gas on timescales similar to the rotation time).

The total amount of gas is difficult to measure at high redshift, and a "reversed" Schmidt Law is sometimes used to determine the amount of gas from the measured SFR (e.g., Péroux et al. 2011). If the starting observation is a surface brightness, then a local law should be used. On the contrary, a global SFR measurement should be combined with a global Schmidtt-Kennicutt. Studying the global law is however not limited to the remote universe. One can see it also as a study of the rate at which the global reservoir of gas in a galaxy becomes available for star formation. In this case, the Schmidt Law is not really a way to study the process of star formation itself, but also the role of gas accretion or other external processes (e.g., Schiminovich et al. 2010).

4.2.3 Which Scale Is Right?

The question of the smallest scale on which the Schmidt Law should be studied is often asked. Koda (2008) suggests that the properties of GMCs provide two limits. The first one is the "drift scale." Young stars have a relative velocity with respect to the gas clouds. In combination with the typical timescale of the star formation tracer used (10 Myr for Hα, 100 Myr for the UV), one can expect a separation between the SFR tracer and the physically related gas of 100 pc–1 kpc. At smaller scales, the SFR tracer and the underlying gas are not physically related. The second scale advocated by Koda (2008) is the separation between GMCs, which is typically 200 pc in the Milky Way, and provide an order of magnitude for other galaxies. The "statistical" behavior of star formation can be seen only if the adopted typical resolution includes at least a few GMCs. Some of the theoretical argument discussed in ❯ Sect. 2 also apply on large scales (e.g., gravitational collapse), up to the kpc scale. Thus, also from this point of view, the Schmidt Law should be valid only on scales larger than at least a few 100 pc.

In their simulations, Feldmann et al. (2011) found that the scatter in the SFR–molecular gas relationship increases rapidly with decreasing averaging scales. In their view, this is due to the fact that the molecular gas is the local "instantaneous" one, while the SFR is time-averaged over 100 Myr timescales.

All these considerations suggest that the Schmidt Law should break down when looking at scales smaller than a few 100 pc and that the scatter should increase when going from the kpc scale downward. Observational work in nearby spirals have recently reached this level (local laws on few 100 pc resolution), and an increase of the scatter of the empirical law when going from the kpc to the 100 pc scales is actually observed (Thilker et al. 2007b; Kennicutt et al. 2007; Bigiel et al. 2008; Verley et al. 2010a; Liu et al. 2011).

4.2.4 Schmidt Laws: Current Observational Status

The left panel of ❯ *Fig. 3-6*, taken from Kennicutt (1998b), shows the Schmidt-Kennicutt Law, with a best fit relation often used in the literature:

$$\Sigma_{\psi} = 2.5\,10^{-4}\left(\frac{\Sigma_{\rm gas}}{1 M_{\odot}\,{\rm pc}^{-2}}\right)^{1.4}. \tag{3.33}$$

It is impressive that this relationship holds on 5 orders of magnitudes of the gas density, showing that there is certainly some level of universality in star formation, related to fundamental processes. Also, the relation is very close (index 1.4 vs. 1.5) to the one proposed in the theoretical section on the simple basis of free fall as the main driver for star formation (❯ 3.10). However, it should be noticed that if one focus on one type of galaxies, e.g., normal spirals, then the scatter remains important, and the slope is not so clearly established. Nevertheless, many other studies have found this relation to give a satisfactory description in many different cases: azimuthal profiles of outer disks (Boissier et al. 2007), tidal dwarf galaxies (Lisenfeld et al. 2001), low surface brightness galaxies and dwarfs (may be with some shift downward with respect to the canonical relation; see, e.g., Boissier et al. 2008; Wyder et al. 2009).

The right part of ❯ *Fig. 3-6* shows that a Schmidt Law including a dynamical factor ($\Omega \propto 1/\tau$) suggested on several theoretical grounds (see ❯ Sect. 2) works as well as the simple Schmidt

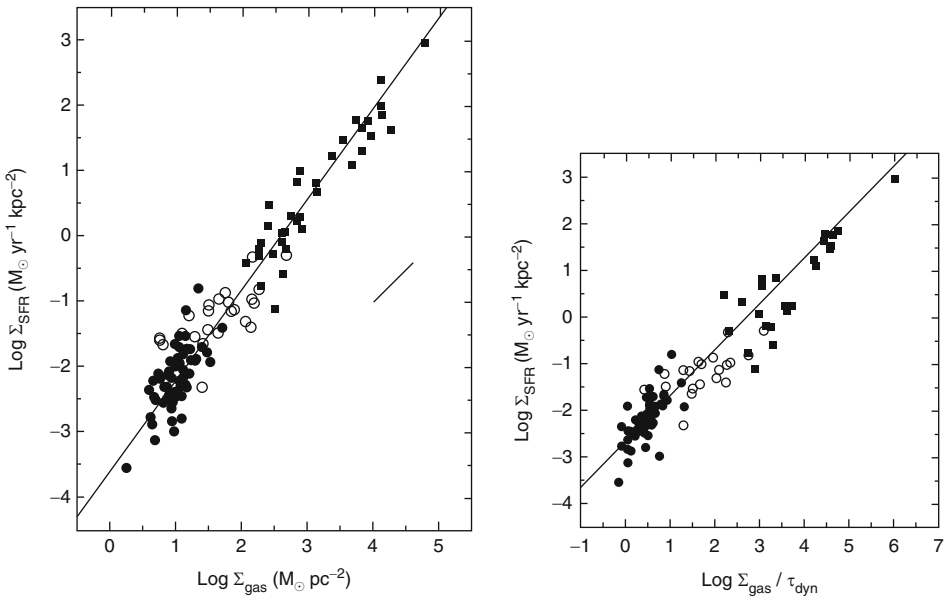

Fig. 3-6

The two panels are reproduced by permission of the AAS from Kennicutt (1998b). On the *left*, the relation between the average SFR and gas surface density is shown. The global Schmidt-Kennicutt Law is valid over 5 orders of magnitudes. On the *right*, a Schmidt Law modulated by a dynamical factor is shown. Both type of laws are in reasonable agreement with the data. The *solid circles* correspond to normal *spirals*, *squares*: circum-nuclear starbursts, *open circles*: central regions of normal disks

Law depending only on the gas density. On this empirical basis, there is no reason to choose one with respect to the other one.[3] The fit by Kennicutt (1998b) for this law is simply

$$\Sigma_\psi = 0.017\Sigma_{\rm gas}\Omega. \tag{3.34}$$

With the advent of high-quality UV data (GALEX satellite) and infrared data (Spitzer), it became recently possible to obtain for large samples of nearby galaxies detailed maps of the SFR (as a combination of UV and far infrared). A noticeable benchmark was obtained by the THINGS team who combined such data with HI and CO maps allowing to proceed to a detailed study of the local Schmidt-Sanduleak Law for a representative sample of spirals and dwarfs (Bigiel et al. 2008; Leroy et al. 2008). Their results are discussed below in quite some details because they represent the state of the art and as such establish a new reference (even if some of their results had been found before on the basis of other samples or methods).

Bigiel et al. (2008) showed that the best local correlation is obtained between the SFR and the molecular gas (see *Fig. 3-7*). Their best fit is

$$\Sigma_\psi = 10^{-2.1\pm0.2}\Sigma_{H_2}^{1\pm0.2}. \tag{3.35}$$

[3] See however the final remark of Sect. 4.2.1

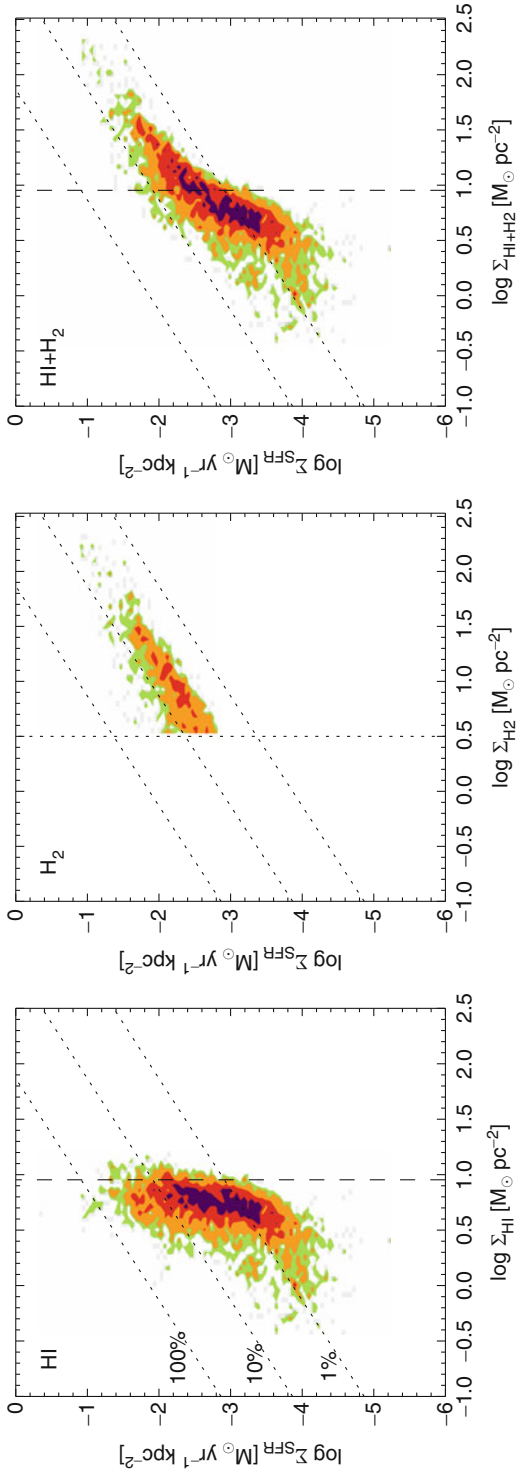

Fig. 3-7
Local Schmidt-Sanduleak Laws observed in Bigiel et al. (2008) for the HI, H2, and total gas (Reproduced with permission of the AAS)

Bigiel et al. (2008) interpret this index $n = 1$ as the fact that several clouds are included within the surface studied at their resolution, and the value of Σ_{H2} is only dictated by the number of clouds within the beam. Then, these clouds all form stars with a universal behavior. There is no clear relation with HI (but a saturation, discussed in Sect. 4.3). The SFR-total gas relation presents a two-slope behavior. At high density, the relation is dominated by the linear relation between the dominant molecular component and the SFR. At low density, it is dominated by the HI/H2 transition. This relation is reproduced in the simple approach of Madore (2010) presented in Sect. 2.3.5. It is also well reproduced by the Krumholz et al. (2009) model (2.3.7), that has been shown to be also in agreement with other observations (e.g., in QSO absorbing systems). This model, however, is purely local (thus it should not be applied to global or azimuthal observations blindly). Krumholz et al. (2009) in fact proposed that, e.g., gravitational instabilities, spiral arms, and other global processes regulate in fact the total gas distribution. Then, their theory predicts the right amount of molecular gas and the SFR.

Leroy et al. (2008) went one step further with respect to the results presented in *Fig. 3-7*. They tried to fit their data with a selection of several possible laws for the transformation of HI into H2 and stars. Despite extensive tests, they could not definitely pinpoint one unique driver for star formation. Many effects are observed (dependence of the ratio $\Sigma_\psi/\Sigma_{\rm gas}$ on the, e.g., radius, orbital timescale, stellar density) but not a single theory can explain the observations over the full range of gas density and in all type of galaxies beyond any doubt. They established that the molecular fraction decreases with radius (what was suggested by previous observations nevertheless) but also with decreasing stellar density, hydrostatic pressure, and orbital timescale (or equivalently Ω). Those dependence are quantified in four scaling relations proposed in their Sect. 5.4.5:

$$\Sigma_{H2}/\Sigma_{HI} = 10.6\exp(-R/0.21R_{25}) \tag{3.36}$$

$$= \Sigma_*/81\mathrm{M}_\odot\,\mathrm{pc}^{-2} \tag{3.37}$$

$$= (P/1.7\,10^4 cm^{-3}Kk_B)^{0.8} \tag{3.38}$$

$$= (\tau_{\rm orb}/1.8\,10^8 yr)^{-2}, \tag{3.39}$$

where R_{25} is the isophotal radius at 25 mag arcsec^2 in the B band and $\tau_{\rm orb}$ is the orbital timescale, thus $\tau_{\rm orb} = 2\pi\Omega^{-1}$.

Note that the dependence on P can be hiding a dependence on the gas density, as already mentioned (see Blitz and Rosolowsky 2006) and that Leroy et al. (2008) did not test relations with "free" index such as (3.23) but only precise relations predicted by various theories (if several phenomenon contribute to the final relation, one can imagine that the final observed relation could be in between the various predictions).

4.2.5 Starbursts and the Schmidt Law

Most of the discussion above concerns spirals and dwarf galaxies. Kennicutt (1998a) included however in his study the circumnuclear starbursts (see *Fig. 3-6*) and found an index 1.4 for the Schmidt-Kennicutt Law. How can this value be reconciled with the linear relation of Bigiel et al. (2008) with H2 (at these high densities, most of the gas is molecular)? Gao and Solomon (2004) proposed that the SFR presents in fact a linear relation with the dense gas density (as traced by HCN) rather than with the molecular content (as traced by CO). In "normal galaxies," the ratio of dense to molecular gas (the dense gas fraction) is constant. Thus, a linear relation is

obtained between the SFR and CO. In starbursts, the SFR is still proportional to the dense gas, but the dense gas fraction becomes larger so that the index n of the Schmidt Law (with either the molecular or the total gas) will be larger than 1. The enhancement in the dense gas fraction in starbursts with respect to normal galaxies has still to find a physical cause, probably linked to the much higher densities and short timescales that they experience (as mentioned in Sect. 2.4). Adding the dependence on the dynamical timescale allow starbursts and normal galaxies to follow a similar relationship, even at high redshift (Genzel et al. 2010; Daddi et al. 2010).

4.3 Observed Thresholds

As seen in Sect. 2.2, various theories for star formation predict the existence of a threshold, or a critical surface density of gas Σ_{crit} below which star formation should not proceed. This motivated several empirical studies, such as the early one of Kennicutt (1989) who observed thresholds in the range 1–10 $M_\odot$ pc^{-2}. Other works suggesting the existence of a sharp threshold followed (Kennicutt 1998b; Martin and Kennicutt 2001), mostly based on Hα azimuthal profiles. A number of more recent works based on another star formation tracer (namely, the UV emission) challenged this view, as star formation (UV emission) was found at very large radius in many nearby galaxies. Boissier et al. (2007) showed that most of the UV azimuthal profiles were extending quite smoothly beyond the optical radius, where it was thought previously that star formation was indeed present but only rare and stochastic (e.g., Ferguson et al. 1998). This UV emission at low density was a very generic finding since the GALEX satellite revealed the existence of so-called XUV (eXtended UV) galaxies (Gil de Paz et al. 2005; Thilker et al. 2005). It was realized little after their discovery that this phenomenon concerns a large fraction of disk galaxies (about 30% according to Thilker et al. 2007a).

Measuring the Hα emission at large radii is quite challenging. Goddard et al. (2010) proposed a new analysis of existing Hα and FUV images for 21 galaxies, computing Hα profiles with an enhanced method (addition of detected object fluxed in radial bins) with respect to simple azimuthal averages. This allowed them to make a detailed comparison of FUV and Hα profiles. They classified their objects into "normal" disks (for which a break is observed in both UV and Hα close to the optical radius) representing 50% of their sample. Note however that a break (change of slope) is observed rather than a very sharp truncation (threshold). The other half of their sample consist in UV extended galaxies. Of these, they claimed that 6 out of 10 galaxies are also extended in Hα, and only 4 out of 10 galaxies have a UV smooth profile and a sharp truncation in Hα.

On a local basis (by opposition to the azimuthal profiles discussed above), the recent work by Bigiel et al. (2008) suggests that there is a (local) critical density for HI, above which the gas is mostly molecular. In other words, there is a saturation of Σ_{HI} around 10 $M_\odot$ pc^{-2} (what had been previously suggested, e.g., Blitz and Rosolowsky 2006). However, the analysis of Leroy et al. (2008) cannot ascribe clearly this "critical density" to any of the threshold theories they tested (Toomre and other). In fact, the saturation corresponds to a phase transition from HI to H2: it does not mean that there should be an absolute threshold for star formation in the total gas density. Although the saturation density seems to favor a Schaye (2004) critical density, Leroy et al. (2008) argue that according to this assumption, the full disk should be supercritical. While it allows to predict an edge for the disk, it does not predict locally within a galaxy the regions forming stars or not.

In conclusion, the idea of a threshold radius beyond which star formation is totally suppressed (and even of a critical density) seems to be of little predictive power to decide where star formation proceeds or not. If there is indeed a gravitational instability threshold corresponding to the full disk being instable and prone to form stars, then beyond the corresponding radius, star formation still proceed, may be due to local enhancements of the density, an idea followed in the simulations of Bush et al. (2008).

Elmegreen and Hunter (2006) proposed that this absence of clear threshold shows that star formation is the results of different processes all combining to produce the observed radial trends. In their view, the SFR saturates at a maximum possible rate independently of the responsible physical process. Especially in outer, low-density regions, this allows to sustain a low level of star formation even when some of these possible processes shut down.

4.4 Relations to the Stellar Content: The Specific Star Formation Rate

The possible influence of the stellar surface density on the SFR surface density was discussed in Sect. 2. Such influence has been studied empirically (e.g., Shi et al. 2011; Abramova and Zasov 2008; Leroy et al. 2008; Dopita and Ryder 1994) but is not clearly favored with respect to other theoretical suggestions. The fact is that a relation seems to exist between the SFR and the stellar mass in the nearby universe (Brinchmann et al. 2004) and at high redshift (Boissier et al. 2010, and references therein). The current interpretation is however that this relation is not causal, but reflects the star formation history of the galaxies.

In fact, the SFR to stellar mass ratio, the specific star formation rate (SSFR), has become an important diagnostic tool to study galaxies (e.g., Buat et al. 2008; Noeske et al. 2007; Bell et al. 2005). The SSFR has the advantage over the SFR to be a normalized quantity, representing the balance between the present activity of a galaxy (the SFR) and its past one (the stellar mass accumulated up to this point). A related quantity is the birthrate parameter b, the current SFR to past average SFR ratio (Kennicutt 1998a). Empirically, it has been directly estimated from the equivalent width of the $H\alpha$ line, and it is also related to broadband colors of galaxies. Salim et al. (2005), for instance, provide a relationship between b and the NUV-r color. Nowadays that stellar mass are relatively easy to estimate, the use of SSFR is more frequent than the one of b. They are however directly related (in a closed box model of evolution with a returned fraction R, age T, SSFR $= b/((1-R)T)$.

The SSFR (or b) is thus an extremely interesting quantity to study galaxy evolution. In the nearby universe, there is a relation between the Hα equivalent width (related to b, see Kennicutt 1998a) and the morphological type (shown in *Fig. 3-8* with the data of James et al. 2004). This relation is due to the differences in the average star formation histories of galaxies of different type as illustrated by the sketch of Sandage (1986a). SSFRs were used also in the context of radial profiles to get clues on the growth history of galactic disks (Muñoz-Mateos et al. 2007) or at high redshift to unravel the mysteries of galaxy formation at the earliest epochs (e.g., Noeske et al. 2007).

4.5 Star Formation History

The SSFR was presented in Sect. 4.4. This quantity gives an important clue on the star formation history of galaxies, but only in a rough sense: the present SFR versus the past averaged

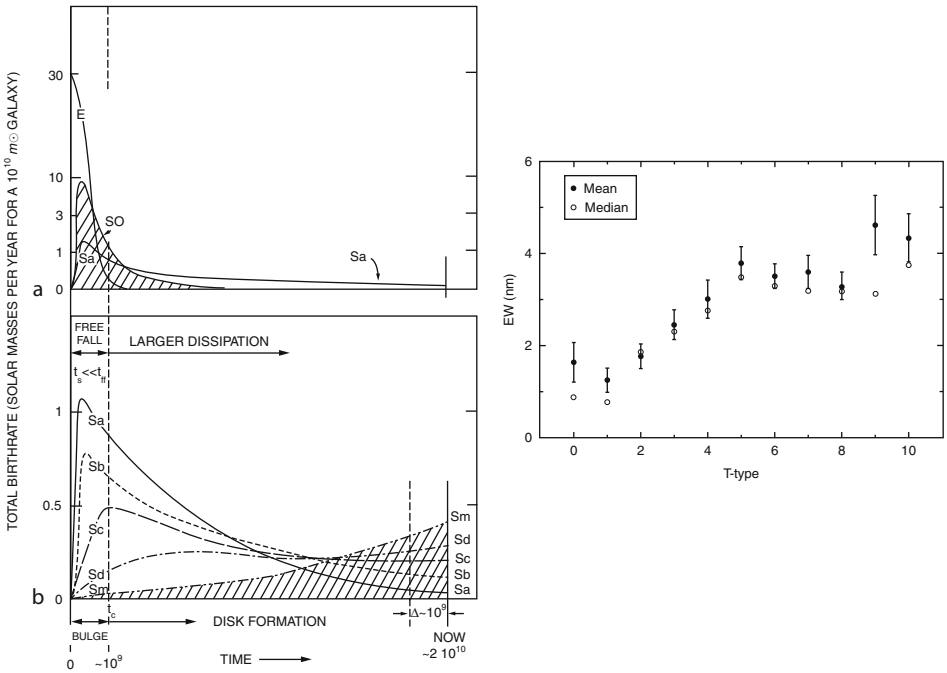

Fig. 3-8

***Left*: Sketch of the average star formation histories of galaxies with various types (taken from Sandage 1986a). Early type are show in panel a and late type galaxies in panel b. Obviously, the *b* parameter (or the SSFR) increases from early to late type. *Right*: Equivalent width of the Hα line (that can be considered as a measure of the birthrate parameter *b*, see Kennicutt 1998a) as a function of type, taken from James et al. (2004) (Credit: Sandage 1986b; James et al. 2004, reproduced with permission ©ESO)**

one. Ideally, to decipher the evolution of galaxies, it is needed to know its star formation history (SFH), i.e. the variation of the SFR with time. In some cases, it is possible to derive it from observations.

An indirect method consist in comparing the predictions of models assuming SFH (e.g., exponentially declining star formation rates or more complex histories) with observational sets. This can be the case for instance of chemical evolution models that are constrained by, e.g., age-metallicity, gas fractions, and metallicity distributions, Spectral synthesis models can be constrained by observed spectra, spectral energy distributions, or simply colors. These indirect methods are not discussed in details here. In the remaining, more direct methods are presented.

In the Milky Way, it is possible to determine the ages of large number of stars. By measuring how many stars are found within bins of ages, it is possible to reconstruct the SFH. One still has to be careful about which component is considered (see, e.g., Wyse 2009): in the thin disk, it is in general assumed (on the basis of observations and chemical evolution models) that the SFR in the solar neighborhood has been oscillating around a more or less constant value, but it should have declined between its early existence and the current epoch if the whole disk is considered. The thick disk and the halo should have different histories according to their formation scenario. Rocha-Pinto et al. (2000) used 552 late-type dwarfs chromospheric ages

to derive a SFH consisting in a series of small amplitude bursts in their 0.4 Gyr bins. Fuchs et al. (2009) used a sample of M-Dwarfs to derive an increase of the Milky Way SFR when going backward in time and compared it to several previous determinations.

Another method consists in the analysis of color-magnitude diagrams (CMDs). Combining the observed position of stars in CMDs with stellar evolution models, it is possible to recover the star formation history of galaxies. This approach has been used in the Milky Way (Hernandez et al. 2000; Cignoni et al. 2006). Especially with the observations of the Hubble Space Telescope, it became possible to resolve stars in many galaxies and apply this method to determine their SFHs. It was found that the local group dwarfs present a large variety in their SFH, with extended episodes of activity separated by short quiescent phases (see, e.g., Tolstoy et al. 2009, and references therein). Harris and Zaritsky (2009) used CMDs in the large magellanic cloud to recover its global SFH, as well as the SFH of various regions within the galaxy.

Of course, comparing the "instantaneous" SFR of galaxies observed at various redshift is another way to derive the history of galaxies (provided it can be assumed that the galaxies observed at various redshifts probe the same population). Nowadays, deep surveys have allowed to measure SFRs in many samples up to relatively large redshifts. Interestingly, a SFR-stellar mass relationship seems to exist (with considerable scatter nevertheless) at all redshifts (see, e.g., the compilation in Boissier et al. 2010), providing an important clue on the history of galaxies (more work is however needed to definitively establish its reallity). In a few studies, SFR measurements have been combined with determinations of the molecular gas content of high-redshift galaxies, what allowed to test the validity of the Schmidt Laws described in Sect. 4.2.4 in the young universe (Bouché et al. 2007; Daddi et al. 2010; Genzel et al. 2010). It was found that a universal Schmidt Law seems to be valid, independently of redshift up to at least $z \sim 2.5$, including both normal and starburst galaxies. The later ones, however, may require a star formation efficiency larger by a factor 4 at high redshift than for $z \sim 0$. It should be kept in mind that uncertainties stay extremely large (for instance, on the H2-CO conversion factor at high redshift) and the number of studies small.

Finally, it is possible to study the evolution with redshift of the "cosmic" SFR, i.e., the SFR per unit volume averaged over very large scales, to obtain a SFR representative of the whole population of galaxies. The famous "Madau plot" shows such a cosmic SFR density as a function of redshift (Madau et al. 1996). Since then, many works have attempted to add points to the diagram and to interpret it. A compilation of measurements of the cosmic SFR density can be found in Hopkins and Beacom (2006), but new observations are added every year from various sources (e.g., galaxies deep surveys, gamma ray bursts). This "cosmic SFR" is to be related to all the other "cosmic" variables that can be obtained trough observations. Wilkins et al. (2008b) compiled measurements of the cosmic stellar mass density as a function of redshift and studied the coherence of the cosmic SFR and stellar mass densities. A related subject is the amount of metals formed by all the generation of stars: an evolution of the "cosmic metallicity" should be found. Metallicity of high-redshift galaxies are measured in QSO or GRB absorbing systems, but are often difficult to relate to the average metallicity on very large scales. Savaglio et al. (2009) show the evolution with reshift of abundances observed in large column density absorbers (for which precise measurements are achievable), but it is unsure that they are representative of the whole population of galaxies. At lower densities, it is possible to place limits on the cosmic metallicity from ionic abundances (e.g., Songaila 2001). Finally, it is possible to link the density of heavy element to the background radiation emitted by the stars responsible for their formation (e.g., Longair 1995, and references therein).

In fact, the cosmic SFR density (and then the related cosmic stellar mass density and cosmic metallicity) is not linked solely to the actual transformation of gas into stars. It is modulated by the SFR distribution and influenced by the whole range of physical processes affecting galaxy evolution (accretion, interactions, feedback, etc.), discussed in more details in the dedicated chapter.

Acknowledgments

It is a pleasure to thank many collaborators with whom I had the chance to discuss various aspects of star formation during the past 10 years, especially Barry Madore and Nikos Prantos. In the process of writing this chapter, I also had stimulating discussions with my colleagues at the Laboratoire d'Astrophysique de Marseille, especially Alessandro Boselli, Véronique Buat, Denis Burgarella, Sébastien Heinis, Olivier Ilbert, and Olga Cucciati. I am thankful for even the shortest discussions we had, and their encouragements. I also thank Jarle Brinchmann who replied to my e-mails instantaneously with clear answers to my questions.

References

Abramova, O. V., & Zasov, A. V. 2008, Astron. Rep., 52, 257
Argence, B., & Lamareille, F. 2009, A&A, 495, 759
Barnes, J. E. 2004, MNRAS, 350, 798
Bastian, N., Covey, K. R., & Meyer, M. R. 2010, ARA&A, 48, 339
Bell, E. F. 2003, ApJ, 586, 794
Bell, E. F., et al. 2005, ApJ, 625, 23
Bicker, J., & Fritze-v. Alvensleben, U. 2005, A&A, 443, L19
Bigiel, F., Leroy, A., Walter, F., Brinks, E., de Blok, W. J. G., Madore, B., & Thornley, M. D. 2008, AJ, 136, 2846
Binney, J., & Tremaine, S. 1987, Galactic Dynamics (Princeton: Princeton University Press)
Blitz, L., & Rosolowsky, E. 2006, ApJ, 650, 933
Boissier, S., & Prantzos, N. 1999, MNRAS, 307, 857
Boissier, S., Prantzos, N., Boselli, A., & Gavazzi, G. 2003, MNRAS, 346, 1215
Boissier, S., et al. 2007, ApJS, 173, 524
Boissier, S., et al. 2008, ApJ, 681, 244
Boissier, S., Buat, V., & Ilbert, O. 2010, A&A, 522, A18+
Boquien, M., Duc, P., Braine, J., Brinks, E., Lisenfeld, U., & Charmandaris, V. 2007, A&A, 467, 93
Boquien, M., et al. 2010a, A&A, 518, L70+
Boquien, M., et al. 2010b, ApJ, 713, 626
Boselli, A., Gavazzi, G., Donas, J., & Scodeggio, M. 2001, AJ, 121, 753
Boselli, A., Boissier, S., Cortese, L., Buat, V., Hughes, T. M., & Gavazzi, G. 2009, ApJ, 706, 1527
Bouché, N., et al. 2007, ApJ, 671, 303
Brinchmann, J., Charlot, S., White, S. D. M., Tremonti, C., Kauffmann, G., Heckman, T., & Brinkmann, J. 2004, MNRAS, 351, 1151
Bronfman, L., Casassus, S., May, J., & Nyman, L. 2000, A&A, 358, 521
Buat, V., & Xu, C. 1996, A&A, 306, 61
Buat, V., et al. 2008, A&A, 483, 107
Buat, V., et al. 2010, MNRAS, 409, L1
Bush, S. J., Cox, T. J., Hernquist, L., Thilker, D., & Younger, J. D. 2008, ApJL, 683, L13
Calzetti, D. 1997, The ultraviolet universe at low and high redshift, in AIP Conf. Ser. 408, ed. W. H. Waller (New York: AIP), 403–412
Calzetti, D., & Kennicutt, R. C. 2009, PASP, 121, 937
Calzetti, D., Kinney, A. L., & Storchi-Bergmann, T. 1994, ApJ, 429, 582
Calzetti, D., et al. 2007, ApJ, 666, 870
Calzetti, D., Sheth, K., Churchwell, E., & Jackson, J. 2009, in The Evolving ISM in the Milky Way and Nearby Galaxies, Chicago
Calzetti, D., et al. 2010, ApJ, 714, 1256
Cassata, P., et al. 2011, A&A, 525, A143+
Chabrier, G., 2003, PASP, 115, 763
Charlot, S., & Fall, S. M. 2000, ApJ, 539, 718
Charlot, S., & Longhetti, M. 2001, MNRAS, 323, 887
Charlot, S., Kauffmann, G., Longhetti, M., Tresse, L., White, S. D. M., Maddox, S. J., & Fall, S. M. 2002, MNRAS, 330, 876
Cignoni, M., Degl'Innocenti, S., Prada Moroni, P. G., & Shore, S. N. 2006, A&A, 459, 783

Condon, J. J. 1992, ARA&A, 30, 575
Corbelli, E. 2003, MNRAS, 342, 199
Cortese, L., Boselli, A., Franzetti, P., Decarli, R., Gavazzi, G., Boissier, S., & Buat, V. 2008, MNRAS, 386, 1157
Cowie, L. L. 1981, ApJ, 245, 66
Cucciati, O., et al. 2012, A&A, 539, 31
Daddi, E., et al. 2010, ApJL, 714, L118
Deharveng, J., et al. 2008, ApJ, 680, 1072
Di Matteo, P., Bournaud, F., Martig, M., Combes, F., Melchior, A., & Semelin, B. 2008, A&A, 492, 31
Dopita, M. A., & Ryder, S. D. 1994, ApJ, 430, 163
Elmegreen, B. G. 1979, ApJ, 231, 372
Elmegreen, B. G. 1993a, in Star Formation, Galaxies and the Interstellar Medium, ed. J. Franco, F. Ferrini, & G. Tenorio-Tagle (Cambridge/New York: Cambridge University Press), 337–348
Elmegreen, B. G. 1993b, ApJ, 411, 170
Elmegreen, B. G., & Hunter, D. A. 2006, ApJ, 636, 712
Feldmann, R., Gnedin, N. Y., & Kravtsov, A. V. 2011, ApJ, 732, 115
Ferguson, A. M. N., Wyse, R. F. G., Gallagher, J. S., & Hunter, D. A. 1998, ApJL, 506, L19
Fuchs, B., Jahreiß, H., & Flynn, C. 2009, AJ, 137, 266
Gallagher, J. S., Bushouse, H., & Hunter, D. A. 1989, AJ, 97, 700
Gao, Y., & Solomon, P. M. 2004, ApJ, 606, 271
Genzel, R., et al. 2010, MNRAS, 407, 2091
Giavalisco, M., Koratkar, A., & Calzetti, D. 1996, ApJ, 466, 831
Gil de Paz, A., et al. 2005, ApJL, 627, L29
Gilbank, D. G., Baldry, I. K., Balogh, M. L., Glazebrook, K., & Bower, R. G. 2010, MNRAS, 405, 2594
Goddard, Q. E., Kennicutt, R. C., & Ryan-Weber, E. V. 2010, MNRAS, 405, 2791
Grimm, H., Gilfanov, M., & Sunyaev, R. 2003, MNRAS, 339, 793
Gronwall, C., et al. 2007, ApJ, 667, 79
Guibert, J., Lequeux, J., & Viallefond, F. 1978, A&A, 68, 1
Harris, J., & Zaritsky, D. 2009, AJ, 138, 1243
Hernandez, X., Valls-Gabaud, D., & Gilmore, G. 2000, MNRAS, 316, 605
Hirashita, H., Buat, V., & Inoue, A. K. 2003, A&A, 410, 83
Hopkins, A. M., & Beacom, J. F. 2006, ApJ, 651, 142
Hopkins, A. M., Connolly, A. J., Haarsma, D. B., & Cram, L. E. 2001, AJ, 122, 288
Hunter, D. A., Elmegreen, B. G., & Baker, A. L. 1998, ApJ, 493, 595
Iglesias-Páramo, J., Boselli, A., Gavazzi, G., & Zaccardo, A. 2004, A&A, 421, 887
Iglesias-Páramo, J., et al. 2006, ApJS, 164, 38
James, P. A., et al. 2004, A&A, 414, 23
Jog, C. J., & Solomon, P. M. 1984, ApJ, 276, 114
Karachentsev, I. D., & Kaisin, S. S. 2010, AJ, 140, 1241
Kennicutt, R. C., Jr. 1989, ApJ, 344, 685
Kennicutt, R. C. 1997, The interstellar medium in galaxies, in Astrophysics and Space Science Library, Vol. 161 (Dordrecht: Astrophysics and Space Science Library), 171–195
Kennicutt, R. C., Jr. 1998a, ARA&A, 36, 189
Kennicutt, R. C., Jr. 1998b, ApJ, 498, 541
Kennicutt, R. C., Jr. et al. 2007, ApJ, 671, 333
Kennicutt, R. C., Jr., Lee, J. C., Funes, José G., S. J., Sakai, S., & Akiyama, S. 2008, ApJS, 178, 247
Kennicutt, R. C., et al. 2009, ApJ, 703, 1672
Kewley, L. J., Geller, M. J., & Jansen, R. A. 2004, AJ, 127, 2002
Koda, J. 2008, Formation and evolution of galaxy disks, in ASP Conf. Ser. 396, ed. J. G. Funes, & E. M. Corsini (San Francisco: Astronomical Society of the Pacific), 97–+
Kong, X., Charlot, S., Brinchmann, J., & Fall, S. M. 2004, MNRAS, 349, 769
Kroupa, P. 2001, MNRAS, 322, 231
Krumholz, M. R., & McKee, C. F. 2008, Nature, 451, 1082
Krumholz, M. R., McKee, C. F., & Tumlinson, J. 2009, ApJ, 699, 850
Larson, R. 1992, in Star Formation in Stellar Systems, ed. G. Tenorio-Tagle, M. Prieto, & F. Sanchez (Cambridge/New York: Cambridge University Press), 125–+
Lee, J. C., et al. 2009, ApJ, 706, 599
Leroy, A. K., Walter, F., Brinks, E., Bigiel, F., de Blok, W. J. G., Madore, B., & Thornley, M. D. 2008, AJ, 136, 2782
Lisenfeld, U., Braine, J., Duc, P., Charmandaris, V., Vallejo, O., Leon, S., & Brinks, E. 2001, in Dwarf Galaxies and Their Environment, ed. K. S. de Boer, R.-J. Dettmar, & U. Klein (Aachen: Shaker), 273–+
Liu, G., et al. 2011, ApJ, 735, 63
Longair, M. S. 1995, in Extragalactic Background Radiation Meeting, ed. D. Calzetti, M. Livio, & P. Madau (Cambridge: Cambridge University Press), 223–236
Luna, A., Bronfman, L., Carrasco, L., & May, J. 2006, ApJ, 641, 938
Madau, P., Ferguson, H. C., Dickinson, M. E., Giavalisco, M., Steidel, C. C., & Fruchter, A. 1996, MNRAS, 283, 1388
Madore, B. F. 1977, MNRAS, 178, 1
Madore, B. F. 2010, ApJL, 716, L131
Madore, B. F., van den Bergh, S., & Rogstad, D. H. 1974, ApJ, 191, 317
Malhotra, S., et al. 2001, ApJ, 561, 766
Martin, C. L., & Kennicutt, R. C., Jr. 2001, ApJ, 555, 301

McKee, C. F., & Ostriker, E. C. 2007, ARA&A, 45, 565
McQuinn, K. B. W., et al. 2010, ApJ, 724, 49
Meurer, G. R., Heckman, T. M., Leitherer, C., Kinney, A., Robert, C., & Garnett, D. R. 1995, AJ, 110, 2665
Meurer, G. R., Heckman, T. M., & Calzetti, D. 1999, ApJ, 521, 64
Mo, M., van den Bosch, F., & White, S. 2009, Galaxies Formation and Evolution (Cambridge: Cambridge University Press)
Monaco, P., Murante, G., Bornagi, S., & Dolag, K. 2012, MNRAS, 421, 2485
Mouhcine, M., Lewis, I., Jones, B., Lamareille, F., Maddox, S. J., & Contini, T. 2005, MNRAS, 362, 1143
Muñoz-Mateos, J. C., Gil de Paz, A., Boissier, S., Zamorano, J., Jarrett, T., Gallego, J., & Madore, B. F. 2007, ApJ, 658, 1006
Muñoz-Mateos, J. C., et al. 2009, ApJ, 701, 1965
Murgia, M., Crapsi, A., Moscadelli, L., & Gregorini, L. 2002, A&A, 385, 412
Noeske, K. G., et al. 2007, ApJL, 660, L47
Osterbrock, D. E., & Ferland, G. J. 2006, Astrophysics of Gaseous Nebulae and Active Galactic Nuclei, ed. D. E. Osterbrock, & G. J. Ferland (Sausalito: University Science Books)
Péroux, C., Bouché, N., Kulkarni, V. P., York, D. G., & Vladilo, G. 2011, MNRAS, 410, 2251
Pflamm-Altenburg, J., Weidner, C., & Kroupa, P. 2007, ApJ, 671, 1550
Quirk, W. J. 1972, ApJL, 176, L9
Ranalli, P., Comastri, A., & Setti, G. 2003, A&A, 399, 39
Robitaille, T. P., & Whitney, B. A. 2010, ApJL, 710, L11
Rocha-Pinto, H. J., Scalo, J., Maciel, W. J., & Flynn, C. 2000, A&A, 358, 869
Rodriguez-Fernandez, N. J., Braine, J., Brouillet, N., & Combes, F. 2006, A&A, 453, 77
Salim, S., et al. 2005, ApJL, 619, L39
Salpeter, E. E. 1955, ApJ, 121, 161
Sandage, A. 1986a, A&A, 161, 89
Sandage, A. 1986b, A&A, 181, 89
Sanduleak, N. 1969, AJ, 74, 47
Savaglio, S., Glazebrook, K., & Le Borgne, D. 2009, ApJ, 691, 182
Schaye, J. 2004, ApJ, 609, 667
Schiminovich, D., et al. 2010, MNRAS, 408, 919
Schmidt, M. 1959, ApJ, 129, 243
Searle, L., Sargent, W. L. W., & Bagnuolo, W. G. 1973, ApJ, 179, 427
Seibert, M., et al. 2005, ApJL, 619, L55
Seigar, M. S. 2005, MNRAS, 361, L20
Shi, Y., et al. 2011, ApJ, 733, 87
Songaila, A. 2001, ApJL, 561, L153
Tamburro, D., Rix, H., Walter, F., Brinks, E., de Blok, W. J. G., Kennicutt, R. C., & Mac Low, M. 2008, AJ, 136, 2872
Tan, J. C. 2000, ApJ, 536, 173
Teyssier, R., Chapon, D., & Bournaud, F. 2010, ApJL, 720, L149
Thilker, D. A., et al. 2005, ApJL, 619, L79
Thilker, D. A., et al. 2007a, ApJS, 173, 538
Thilker, D. A., et al. 2007b, ApJS, 173, 572
Tolstoy, E., Hill, V., & Tosi, M. 2009, ARA&A, 47, 371
Toomre, A. 1964, ApJ, 139, 1217
van den Bergh, S. 1999, A&AR, 9, 273
Verley, S., Corbelli, E., Giovanardi, C., & Hunt, L. K. 2010a, A&A, 510, A64+
Verley, S., et al. 2010b, A&A, 518, L68+
Wang, B., & Silk, J. 1994, ApJ, 427, 759
Weilbacher, P. M., & Fritze-v. Alvensleben, U. 2001, A&A, 373, L9
Whitney, B. A., et al. 2008, AJ, 136, 18
Wilkins, S. M., Hopkins, A. M., Trentham, N., & Tojeiro, R. 2008a, MNRAS, 391, 363
Wilkins, S. M., Trentham, N., & Hopkins, A. M. 2008b, MNRAS, 385, 687
Wong, T., & Blitz, L. 2002, ApJ, 569, 157
Wyder, T. K., et al. 2009, ApJ, 696, 1834
Wyse, R. F. G. 1986, ApJL, 311, L41
Wyse, R. F. G. 2009, in IAU Symp., Vol. 258, ed. E. E. Mamajek, D. R. Soderblom, & R. F. G. Wyse, 11–22
Wyse, R. F. G., & Silk, J. 1989, ApJ, 339, 700